Faculty of Physics and Astronomy
University of Heidelberg

Diploma thesis

in Physics

submitted by Babette Minna Wilhelmine Döbrich

born in Munich, Germany

March 2008

Non-perturbative access to Casimir-Polder potentials in nontrivial geometries

This diploma thesis has been carried out by Babette Döbrich

at the Physikalisches Institut

under the supervision of Priv.-Doz. Dr. Maarten DeKieviet

Abstract

A Quantum Field Theoretical treatment of fluctuating fields in the presence of boundaries is reviewed and applied to Casimir-Polder type problems. The focus of the investigations lies on the calculation of the fluctuation-induced potential for the case of arbitrarily shaped surfaces. We discuss two possible non-perturbative calculation schemes. First, the standard Casimir-Polder result for an atom in front of a conducting plane is rederived within the field theoretical treatment through the use of a thinning process, and possible extensions to structured surfaces are discussed. The second approach considers the induced potentials of a Dirichlet scalar field in the case of a sphere-surface configuration. We calculate the potential in the limit of a flat plane and derive an expression for the Casimir energy that allows for an easy numerical evaluation of the potential in cases of uniaxially corrugated surfaces. Finally we present numerical results on the Casimir-Polder potential for a one-dimensional sinusoidal corrugation.

Ein Überblick über die Beschreibung fluktuierender Felder unter Einfluss externer Randbedingungen wird gegeben und auf die Behandlung von Casimir-Polder Problemen angewendet. Der Schwerpunkt der Betrachtungen liegt auf der Berechnung fluktuationsinduzierter Potenziale für nichtplanare Oberflächen. Wir betrachten zwei nichtperturbative Berechnungsschemata. Zunächst wird die gewöhnliche Casmir-Polder Formel für ein Atom vor einer flachen Leiteroberfläche im Rahmen des Formalismus durch einen Ausdünnungsprozess hergeleitet und die Erweiterung auf strukturierte Oberflächen wird diskutiert. Anschliessend werden die induzierten Energien für ein skalares Dirichlet Feld in einer Kugel-Platte Anordnung besprochen. Wir berechnen das Potenzial im Falle einer flachen Platte und leiten einen Ausdruck her, der eine einfache Bestimmung der Casimir-Polder Kräfte für uniaxial strukturierte Oberflächen erlaubt. Zuletzt präsentieren wir numerische Resultate für den Fall einer eindimensionalen, sinusoidalen Korrugation.

Contents

1 Introduction

The general notion of vacuum is just a volume purged of particles. In classical physics, nothing interesting is expected to happen there.

In contrast, when speaking of a quantum vacuum, basically two effects come into play that belong to the cornerstones of modern physics. Roughly spoken we know, thanks to Heisenberg, that energy can fluctuate considerably over short instances of time. These fluctuations can, according to Einstein, manifest themselves as particles, which previously were not there. It is possible to disturb these fluctuations systematically in order to test and extend our knowledge of the physical laws that hold in these systems. Thus, the classical notion of vacuum is overthrown and a vast field of new phenomena opens up for inspection.

Consider, for example, two infinitely large and ideally conducting surfaces that are aligned in parallel in vacuum at zero temperature. Photons that emerge between the plates have to obey certain boundary conditions dictated by Maxwell's equations. The allowed number of fluctuation modes is thus restricted in between the surfaces whilst on the outside the number of permissible modes is higher.

For these reasons, we expect an attractive force between two plates separated by a distance of H. The first analytical computation for this configuration was performed by the Dutch physicist Hendrik Brugt Casimir in 1948 [1]. He predicted that those plates attract each other with a force per unit plate area of[1]

$$\mathcal{F} = -\frac{\pi^2}{240}\frac{\hbar c}{H^4} \ . \tag{1.1}$$

What preceded this ground-breaking result was a calculation that Casimir had done together with Dirk Polder earlier in the same year [4]. Inspired by a disagreement between experimental results and theoretical predictions in context of the interaction between colloidal particles, Casimir and Polder accounted for the effect of retardation in the London-van der Waals forces. By means of perturbative Quantum Electrodynamics they found that a neutral atom located at a distance r in front of a perfectly conducting plane is subject to an interaction potential $\sim \frac{1}{r^3}$ in the non-retarded regime, whereas in the retarded regime the interaction falls of more quickly $\sim \frac{1}{r^4}$. The limit of both regimes is included in an empirical formula for the Casimir-Polder potential

[1] Note that though this force quickly decreases with larger distances, for parallel plates $\mathcal{F}$ amounts to an equivalent of approximately one atmospheric pressure at a separation of about ten nanometers. The first experimental verifications of the Casimir force, however, were done in the easier accessible configuration of a sphere and a flat plate [2, 3].

which can be written as

$$V(r) = -\frac{C_4}{r^3(r+l)} \ , \tag{1.2}$$

with l being the wavelength of the dominant dipole transition of the atom and C_4 a potential strength parameter.

Motivated by a discussion[2] with Niels Bohr, Casimir then rederived his result in a notably simpler way through the consideration of the shift in zero point energy induced by the sheer presence of the atom and the plane [6]. Later he published his famous prediction for the case of parallel conducting planes as described above and thereby founded a whole new area of research.

Nowadays forces that arise when quantum or classical[3] fluctuations are restricted by boundaries generally run under the name of Casimir forces. Those forces play a role in very distinct research areas ranging from cosmology to biology and on to engineering[4]. They therefore invoke increasing interest among experimentalists and theoreticians.

Extensive research on the subject of Casimir and Casimir-Polder forces is now done on the correction and extension of Eqs. (1.1) and (1.2) for more realistic conditions including e.g. non-zero temperature, finite conductivity, edge effects, and so forth. For general reviews on the subject, see for example [5, 10, 11, 12, 13, 14].

In particular, the aim of this thesis is to get a better quantitative handle on the *geometrical* implications of Casimir-Polder forces.

However, one should not be lead by the beautifully simple expressions of (1.1) and (1.2) to believe that a generalization of these results to nontrivially shaped boundaries is an easy task. Since the forces for flat segments are well-known, it would seem to be a good starting point to just divide the arbitrarily shaped objects into small segments and sum over the forces that act between them when the curvature of the objects is small compared to their separation.

Yet in fact fluctuation induced forces are inherently non-additive. Therefore this is an approximation which often does not do justice to the experimental results. Going beyond this method known as Proximity Force Ap-

[2]Discussion maybe is not quite the right word. It is passed down from Casimir's notes that Bohr only mumbled something about the connection to zero point energy [5]. But already this put Casimir on the right track.

[3]A classical Casimir force can for example emerge from density fluctuations in liquids [7] and has only recently been directly observed [8].

[4]Since at the nano scale Casimir interactions become the dominant force for uncharged conductors, a good understanding of these forces is needed in the fast-developing field of Micro-Electro-Mechanical Systems (MEMS) [9].

proximation (PFA) [15, 16] is therefore desired and advanced by the Casimir community by the use of various techniques [17, 18, 19, 20, 21, 22, 23, 24, 25].

In particular, recent experimental results on Casimir-Polder potentials for nano-structured surfaces induced us to study the possibilities of predicting these interactions for nontrivial geometries.

In the Atomic Beam Spin Echo (ABSE)-apparatus here in Heidelberg,^{3}He-atoms were quantum reflected [26, 27] from the attractive Casimir-Polder potential between an atom and a structured plate [28]. Of particular interest are the empirical potentials thus found for an aluminum sawtooth structure.

Adapting the notation of Eq. (1.2), the potentials could be written as

$$V(r) = -\frac{C_n}{r^{n-1}(r+l)} \ , \tag{1.3}$$

which were extracted for three different orientations of the incident beam with respect to the periodic structure.

It was observed that the power n with which the potential decreases depends on the incident angle of the atomic beam in the following way:

- along the ridges $n = 6$
- orthogonal to the ridges $n = 5$
- under a 45 degree angle with respect to the ridges $n = 4$.

So far, there are no theoretical predictions ready to be compared to these results. In order to consider geometrical implications of Casimir-Polder forces, methods of pairwise summation [29] or perturbative approximations [30] can be used.

However, in the ABSE-scattering experiments interaction regions are probed where the distance between the atom and the plate becomes comparable to the height of the sawteeth. Casimir-Polder calculations based on perturbative approximations are therefore inapt for comparison with this data and non-perturbative methods have to be reviewed and extended.

2 Casimir forces for scalar fields

2.1 Scalar field theory with boundaries

In the functional integral formulation of a Quantum Field Theory, almost all quantities of interest can be extracted from a generating functional $\mathcal{Z}$. This is also true for Casimir forces between surfaces. Let us elaborate on this first in the simplest scenario of a real-valued massless scalar field.

2.1.1 Casimir energy from a restricted partition function

In Euclidean QFT, $\mathcal{Z}$ for a massless scalar field ϕ in the absence of external sources is defined as

$$\mathcal{Z} = \int \mathcal{D}\phi \exp(-S_E[\phi]) \quad , \tag{2.1}$$

where after a Wick rotation[5] to imaginary time the Euclidean action reads $S_E = \frac{1}{2}\int d^4x \left(\partial\phi(x)\right)^2$. Basically, in order to find the Casimir energy of a system containing fluctuation boundaries, we have to calculate the ground state energy of this system with the respective fluctuation restrictions accounted for. Since this energy is infinite, the fluctuation-induced energy of the system without boundaries has to be subtracted to obtain a finite-valued result.

For these reasons, the Casimir energy of a system bounded by two plates at (mean) separation H is obtained by solving

$$E_{cas}(H) = -\frac{\hbar c}{T_E} \ln \frac{\mathcal{Z}_{B.C.}}{\mathcal{Z}_\infty} \ , \tag{2.2}$$

where $\mathcal{Z}_{B.C.}$ stands for the generating functional of the fluctuating field obeying the system's boundary conditions, whereas $\mathcal{Z}_\infty$ represents the case of infinite separation between the objects (i.e. $H \to \infty$). T_E is the overall length in Euclidean time direction which drops out upon the evaluation of the logarithm as we will see shortly.

The force between the surfaces is consequently given by

$$F_{cas}(H) = \frac{\hbar c}{T_E} \partial_H \ln \frac{\mathcal{Z}_{B.C.}}{\mathcal{Z}_\infty} \ . \tag{2.3}$$

The implementation of the boundary conditions for the fields can be achieved via the insertion of a δ-functional into $\mathcal{Z}$ which forces the fields to behave correctly on the surfaces. This method was first applied to Casimir-type problems in [31].

[5] This implies for the time variable a rotation of $t \to t_\mathrm{E}/\imath$, where t_E is called the Euclidean time.

2.1.2 Dirichlet boundary conditions

Consider, for example, the most simple case of a fluctuating scalar field obeying Dirichlet (D) boundary conditions on the surfaces. The Dirichlet boundary conditions are simply $\phi(x_\alpha) = 0$ for a 4-vector x_α pointing onto a surface S_α, with α labeling different disjoint surfaces.

Hence, $\mathcal{Z}_{B.C.}$ in the case of two plates case is given by

$$\mathcal{Z}_D = \frac{1}{\mathcal{Z}_0} \int \mathcal{D}\phi \prod_{\alpha=1}^{2} \prod_{x_\alpha} \delta\left(\phi(x_\alpha)\right) \exp\left(-S_E\right) \ , \tag{2.4}$$

where $\mathcal{Z}_0$ is a normalization factor of which we will make use later.

Now, in order to evaluate the integral over the fields, the δ-functional can be rewritten as its functional Fourier transform with the help of auxiliary fields ψ_α "living" on the plates [31, 32, 33, 34, 35]. This implies that they vanish for all space-time points that do not lie on the plates .

Thus, using

$$\prod_{x_\alpha} \delta\left(\phi\left(x_\alpha\right)\right) = \int \mathcal{D}\psi_\alpha \exp\left(\imath \int_{S_\alpha} dx_\alpha \psi_\alpha(x_\alpha)\phi(x_\alpha)\right) \ , \tag{2.5}$$

Eq. (2.4) now reads:

$$\mathcal{Z}_D = \frac{1}{\mathcal{Z}_0} \int \mathcal{D}\phi \prod_{\alpha=1}^{2} \int \mathcal{D}\psi_\alpha \exp\left(\imath \int_{S_\alpha} dx_\alpha \psi_\alpha(x_\alpha)\phi(x_\alpha)\right) \times \exp\left(-\frac{1}{2}\int d^4x (\partial\phi(x))^2\right) \ . \tag{2.6}$$

After rewriting the integral over the surfaces in the exponential in terms of a 4-volume integral via

$$\int_{S_\alpha} dx_\alpha \psi_\alpha(x_\alpha)\phi(x_\alpha) = \int d^4x \left[\int_{S_\alpha} dx_\alpha \delta^{(4)}(x - x_\alpha)\psi_\alpha(x_\alpha)\right] \phi(x) \ , \tag{2.7}$$

the square in $\phi(x)$ in the exponential function can be completed and the Gaussian integration $\int \mathcal{D}\phi$ can be carried out. The numerical value of the integral is absorbed into the normalization $\mathcal{Z}_0$, which accounts for the value of the integral over the unrestricted fields.

The physics of the system is then contained in

$$\mathcal{Z}_D = \prod_{\gamma=1}^{2} \int \mathcal{D}\psi_\gamma(x_\gamma) \exp\left[-\frac{1}{2}\sum_{\alpha,\beta} \int_{S_\alpha}\int_{S_\beta} dx_\alpha dx_\beta \psi_\alpha(x_\alpha) G(x_\alpha, x_\beta)\psi_\beta(x_\beta)\right] \ , \tag{2.8}$$

where $G(x_\alpha, x_\beta)$ is the functional inverse of ∂^2 evaluated on the plates. For four-vectors x and x', it is simply given by

$$G(x, x') = \frac{1}{4\pi^2} \frac{1}{(x - x')^2} \ . \tag{2.9}$$

Now all that remains is another Gaussian integration in terms of the auxiliary fields on the plates. Defining a matrix $\mathcal{M}$ with elements

$$\mathcal{M}_{\alpha\beta} = G(x_\alpha, x_\beta) \ , \tag{2.10}$$

$\mathcal{Z}_D$ becomes

$$\mathcal{Z}_D = (\det \mathcal{M})^{-\frac{1}{2}} \tag{2.11}$$

and thus one finds

$$\ln \mathcal{Z}_D = -\frac{1}{2} \mathsf{tr} \ln \mathcal{M} \ . \tag{2.12}$$

Note that the determinant and the trace in Eqs. (2.11) and (2.12) have to be evaluated with respect to the discrete plate indices as well as the continuous space-time variables. Furthermore it should be emphasized that the space-time integration still runs over the surfaces[6].

Now consider again the expressions for the Casimir potential and force: Eqs.(2.2) and (2.3). One sees that fluctuations not contributing to the Casimir force are removed by the subtraction of the generating functional for infinite plate-plate separation $\mathcal{Z}_\infty$.

By the calculations of the previous lines we now know that we can rewrite the ratio of the restricted and unrestricted generating functionals as

$$\ln \frac{\mathcal{Z}_{B.C.}}{\mathcal{Z}_\infty} = -\frac{1}{2} \mathsf{tr} \ln \frac{\mathcal{M}}{\mathcal{M}_\infty} \ . \tag{2.13}$$

Thus, combining the result of Eq. (2.13) with (2.2) and (2.3), the Casimir energy and force are finally given by

$$\begin{aligned} E_{cas}(H) &= \frac{\hbar c}{T_E} \frac{1}{2} \mathsf{tr} \ln \frac{\mathcal{M}}{\mathcal{M}_\infty} \\ F_{cas}(H) &= -\frac{\hbar c}{T_{\mathrm{E}}} \partial_H \frac{1}{2} \mathsf{tr} \ln \frac{\mathcal{M}}{\mathcal{M}_\infty} \ . \end{aligned} \tag{2.14}$$

In a system with only two surfaces as we will consider in the following, the matrices determining the force explicitly read:

$$\mathcal{M} = \begin{pmatrix} \mathcal{M}_{11} & \mathcal{M}_{12} \\ \mathcal{M}_{21} & \mathcal{M}_{22} \end{pmatrix} \tag{2.15}$$

[6]Note that this definition thus for example deviates from the quantity Γ as used in [32].

and

$$\mathcal{M}_\infty = \begin{pmatrix} \mathcal{M}_{11} & 0 \\ 0 & \mathcal{M}_{22} \end{pmatrix} . \tag{2.16}$$

Note that the same calculational steps in principle also apply for Neumann boundary conditions. The functional δ enforcing appropriate boundary condition then reads

$$\delta\left(\partial_n \phi(x_\alpha)\right) = 0 , \tag{2.17}$$

and the matrix elements of (2.14) are then given in terms of derivatives of the Green's functions along the normal vectors of the surfaces:

$$\mathcal{M}_{\alpha\beta} = \partial_{n_\alpha} \partial_{n_\beta} G(x_\alpha, x_\beta) . \tag{2.18}$$

2.2 The flat plate scenario

2.2.1 Prerequisites

To get acquainted with the calculational steps that will be applied throughout the thesis, we want to elaborate on the simplest thinkable scenario. We present the case of two ideally conducting plates that are aligned in parallel and separated by a distance H in order to reproduce Casimir's celebrated result as given in Eq. (1.1).

This result of course considers the effect of electromagnetic interactions, but for the case of two translationally invariant spatial directions, namely the directions along the plates, the calculation can be performed in terms of two scalar fields obeying Dirichlet and Neumann boundary conditions, respectively. This remains true even for only one translationally invariant direction, i.e. uniaxially corrugated, ideally conducting surfaces.

To see this, one has to check that due to the symmetry of the problem the initially six independent components of the electric and magnetic field in fact can all be expressed in terms of two field components. This phenomenon is well known from cylindrical waveguides [36]. As in the context of waveguides, the independent field components are called transversal electric (TE) and transversal magnetic (TM) modes and consequently the fields are labeled ϕ_{TE} and ϕ_{TM}.

Furthermore we note that for the case of flat plates the TE and TM modes contribute equally to the Casimir force due to the symmetry of the setup. Therefore the result of the calculation for only one scalar field just has to be multiplied by a factor of two in order to obtain the correct value of the force. This, however, is not longer true for non-planar surfaces and makes

the calculation for uniaxially corrugated surfaces hard, though a calculation in terms of scalar fields is allowed.

In order to be able to evaluate the trace of the logarithm as given in Eq. (2.14), we expand the logarithm into a series. For the trivial case of parallel plates it will - as one expects - turn out, that the series terms are resummable after the trace has been evaluated and yield the well-known analytical result. For nontrivial geometries this will not be possible and in principle infinitely many terms would have to be taken into account in order to obtain exact results.

For Casimir-Polder type problems though, the calculation will break down to the evaluation of just one term of the logarithmic series. This obviously reduces the calculational effort immensely. We will come to this in the next chapters and explain how this comes about.

Now, as a first step in order to expand the logarithm in the expression for the Casimir energy (2.14), we rewrite its argument as

$$\mathcal{M}\mathcal{M}_\infty^{-1} = \begin{pmatrix} 1 & \mathcal{M}_{11}^{-1}\mathcal{M}_{12} \\ \mathcal{M}_{22}^{-1}\mathcal{M}_{21} & 1 \end{pmatrix} = \mathbf{1} + \Delta\mathcal{M} \ , \tag{2.19}$$

where we define the quantities:

$$\Delta\mathcal{M} \equiv \begin{pmatrix} 0 & \Delta\mathcal{M}_{12} \\ \Delta\mathcal{M}_{21} & 0 \end{pmatrix} \equiv \begin{pmatrix} 0 & \mathcal{M}_{11}^{-1}\mathcal{M}_{12} \\ \mathcal{M}_{22}^{-1}\mathcal{M}_{21} & 0 \end{pmatrix} \ . \tag{2.20}$$

We can thus rewrite the trace log expression appearing in (2.14) as

$$\frac{1}{2}\mathsf{tr}\ln\frac{\mathcal{M}}{\mathcal{M}_\infty} = \mathsf{tr}\left(\sum_{n=1}^{\infty}\frac{(-1)^{n-1}}{2n}\Delta\mathcal{M}^n\right) \ . \tag{2.21}$$

Obviously, due to the off-diagonal structure of $\Delta\mathcal{M}$, terms with odd n do not contribute since the trace vanishes there.

Note again that the trace is to be understood as the trace over the matrix elements and the trace over the internal indices of the matrices $\Delta\mathcal{M}_{12}$ and $\Delta\mathcal{M}_{21}$.

Consequently, it remains to evaluate

$$\frac{1}{2}\mathsf{tr}\ln\frac{\mathcal{M}}{\mathcal{M}_\infty} = \sum_{n=1}^{\infty}\frac{-1}{4n}\mathsf{tr}\left((\Delta\mathcal{M})^{2n}\right) \ , \tag{2.22}$$

where $(\Delta\mathcal{M})^2$ by definition is a diagonal matrix:

$$(\Delta\mathcal{M})^2 = \begin{pmatrix} \Delta\mathcal{M}_{12}\Delta\mathcal{M}_{21} & 0 \\ 0 & \Delta\mathcal{M}_{21}\Delta\mathcal{M}_{12} \end{pmatrix} \ . \tag{2.23}$$

Therefore Eq. (2.14) now reads

$$\begin{aligned} E_{cas}(H) &= -\frac{\hbar c}{T_{\mathrm{E}}}\sum_{n=1}^{\infty}\frac{1}{4n}\mathsf{tr}\left((\Delta\mathcal{M})^{2n}\right) \\ F_{cas}(H) &= \frac{\hbar c}{T_{\mathrm{E}}}\sum_{n=1}^{\infty}\frac{1}{4n}\partial_H\mathsf{tr}\left((\Delta\mathcal{M})^{2n}\right) \ . \end{aligned} \tag{2.24}$$

Taking into account the cyclicity of the trace we see that the necessary ingredient for the calculation of the Casimir energy and force is given by the term

$$\mathsf{tr}\left(\Delta\mathcal{M}_{12}\Delta\mathcal{M}_{21}\right) = \mathsf{tr}\left(\mathcal{M}_{11}^{-1}\mathcal{M}_{12}\mathcal{M}_{22}^{-1}\mathcal{M}_{21}\right) \tag{2.25}$$

and the corresponding traces of higher powers.

We would like to mention that this expression furthermore provides a nice physical picture of what actually is computed to obtain the fluctuation-induced forces: Starting from a generic point y on surface S_1, it is summed over all possible propagations on the surface itself, followed by all possible propagations to the second surface S_2, then generic propagations on S_2 itself and all thinkable ways back to S_1 again. At last it is summed over all possible starting points y. A *cycle* of induced propagations so to say[7].

To see this more clearly one should not forget that the products in (2.25) are only short-hand notation for the value of the integrations over the two surfaces. Thus, Eq. (2.25) in the case of two *flat* surfaces reads

$$\begin{aligned} &\int_{\underline{x}}\int_{\underline{x}'}\int_{\underline{x}''}\int_{\underline{x}'''} \\ &\times\,\mathcal{M}_{11}^{-1}(\underline{x},\underline{x}')\mathcal{M}_{12}(\underline{x}',\underline{x}'')\mathcal{M}_{22}^{-1}(\underline{x}'',\underline{x}''')\mathcal{M}_{21}(\underline{x}''',\underline{x})\big|_{x_3,x_3'=0;x_3'',x_3'''=H} \ . \end{aligned} \tag{2.26}$$

Here and from here on, we have changed the notation from x_α to $x = (x_0, x_1, x_2, x_3) = (\underline{x}, x_3)$ and are thus suppressing the surface index on the four-vectors for clarity. We have done this in order to not confuse the surface index with the index referring to the component of the four-vector. The x_3-component is evaluated on the surfaces and only an integration over the time direction and the two directions along the plates remain (i.e. along $\underline{x}$).

[7] In Casimir problems, any order of successive cycles contributes to the overall potential. However, as already mentioned, we will see that for Casimir-Polder problems the calculation of only one of these cycles suffices. This is related to the fact that in a Casimir-Polder problem the dimensionality of one surface is reduced and therefore propagations on this surface do not contribute.

2.2.2 Position space

Let us now derive the expressions needed for the calculation of the propagation cycle in Eq. (2.25) explicitly. Even though the calculation is by far easier in momentum space (see section 2.2.3), the coordinate space calculation generalizes more straight forwardly to non-planar surfaces. Therefore the expressions derived here will come in handy in section 4, where we will consider the propagators in the setup of a planar surface and a sphere.

The functional inverse of $\mathcal{M}_{11}$ and $\mathcal{M}_{22}$ on a flat surface is just the operator $\mathcal{D}$ which, for $\underline{x} = (x_0, x_{1,}, x_2)$, satisfies:

$$\mathcal{D}\left(\frac{1}{4\pi^2 \underline{x}}\right) = \delta(\underline{x}) \ . \tag{2.27}$$

The solution to Eq. (2.27) is

$$\mathcal{D} = 2\sqrt{-\nabla^2} \ , \tag{2.28}$$

where $\nabla = (\partial_0, \partial_1, \partial_2)$.

With $\mathcal{M}_{11}^{-1}$ given and the propagator between the plates

$$\mathcal{M}_{12}(\underline{x} - \underline{x}') = \frac{1}{4\pi^2} \frac{1}{(\underline{x} - \underline{x}')^2 + H^2} \ , \tag{2.29}$$

we can now easily calculate

$$\Delta\mathcal{M}_{12}(\underline{x} - \underline{x}') = \frac{1}{\pi^2} \frac{H}{(H^2 + (\underline{x} - \underline{x}')^2)^2} \ . \tag{2.30}$$

Integrating now over the coordinates on the second surface we find the following expression for a full cycle of propagations:

$$\left[\Delta\mathcal{M}_{12}\Delta\mathcal{M}_{21}\right](\underline{x} - \underline{x}') = \frac{2}{\pi^2} \frac{H}{(4H^2 + (\underline{x} - \underline{x}')^2)^2} \tag{2.31}$$

and thereby, upon further integrations, in principle $\mathsf{tr}\left(\Delta\mathcal{M}^{2n}\right)$ for all n.

For an explicit demonstration of the derivation of Eqs. (2.28 - 2.31), please refer to Appendix A.

The respective terms of the sum

$$\sum_{n=1}^{\infty} \frac{1}{4n} \mathsf{tr}\left(\Delta\mathcal{M}^{2n}\right) = \frac{1}{4}\mathsf{tr}(\Delta\mathcal{M}^2) + \frac{1}{8}\mathsf{tr}(\Delta\mathcal{M}^4) + \frac{1}{12}\mathsf{tr}(\Delta\mathcal{M}^6) + \dots \ , \tag{2.32}$$

can now, using (2.31), be explicitly evaluated. One finds

$$\sum_{n=1}^{\infty} \frac{1}{4n} \mathsf{tr}\left(\Delta \mathcal{M}^{2n}\right) = \frac{1}{4}\left(\frac{1}{4}\frac{1}{\pi^2 H^3} T_E A\right) + \frac{1}{8}\left(\frac{1}{32}\frac{1}{\pi^2 H^3} T_E A\right) + \frac{1}{12}\left(\frac{1}{108}\frac{1}{\pi^2 H^3} T_E A\right) + \dots \ , \quad (2.33)$$

with surface area A and length in Euclidean time direction T_E.

The numerical factors can then be regrouped in the following way:

$$\sum_{n=1}^{\infty} \frac{1}{4n} \mathsf{tr}\left(\Delta \mathcal{M}^{2n}\right) = \left(1 + \frac{1}{16} + \frac{1}{81} + ...\right)\left(\frac{1}{16}\frac{1}{\pi^2 H^3} T_E A\right) \ , \quad (2.34)$$

where the convergent sum $\sum_{n=1}^{\infty} \frac{1}{n^4} = \frac{\pi^4}{90}$ appears as can be proved by induction.

Thus we arrive at

$$\sum_{n=1}^{\infty} \frac{1}{4n} \mathsf{tr}\left(\Delta \mathcal{M}^{2n}\right) = \frac{T_E A}{1440}\frac{\pi^2}{H^3} \ . \quad (2.35)$$

Finally, using (2.24), we find for the contribution of the transversal electric modes to the Casimir force between the plates $F_{\mathrm{TE}} = -\frac{\hbar c A}{480}\frac{\pi^2}{H^4}$. Remembering that we have to take into account also the transversal magnetic modes of the fluctuating field which contribute by the same amount, we finally arrive at the force density:

$$\mathcal{F}_{cas} = -\frac{\pi^2}{240}\frac{\hbar c}{H^4} \ , \quad (2.36)$$

as expected (cf. Eq. (1.1)).

2.2.3 Momentum space

In cases where translational symmetry is given along one or more directions of x, though, it is favourable to perform the calculation in momentum space with respect to those components. The reason for this is the well-known fact that the matrix elements $\mathcal{M}_{\alpha\beta}$ become diagonal in their momentum if they depend only on the difference of their arguments in position space.

Here, apparently the time direction and the two lateral space-directions are translationally invariant.

We again start with the force as given in Eq. (2.14):

$$F_{cas}(H) \ = -\frac{\hbar c}{T_{\mathrm{E}}}\partial_H \frac{1}{2}\mathsf{tr}\ln\frac{\mathcal{M}}{\mathcal{M}_\infty} \ . \quad (2.37)$$

Using the Fourier transform of (2.31):

$$[\Delta\mathcal{M}_{12}\Delta\mathcal{M}_{21}]\,(|\underline{p}|) = \exp(-2Hp)\ , \tag{2.38}$$

where $p = |\underline{p}|$, we find that we do not even have to expand the logarithm to obtain the analytical value for the force.

This can be seen as follows: As before we define

$$\frac{1}{2}\mathsf{tr}\ln\frac{\mathcal{M}}{\mathcal{M}_\infty} = \frac{1}{2}\mathsf{tr}\ln(\mathbf{1}+\Delta\mathcal{M})\ . \tag{2.39}$$

Considering now that due to the off-diagonal structure of the matrices $\Delta\mathcal{M}$ as defined in (2.20), the traces over odd powers of $\Delta\mathcal{M}$ vanish and it therefore holds that

$$\frac{1}{2}\mathsf{tr}\ln(\mathbf{1}+\Delta\mathcal{M}) = \frac{1}{4}\mathsf{tr}\ln(\mathbf{1}-\Delta\mathcal{M}^2) = \frac{1}{2}\mathsf{tr}\ln(\mathbf{1}-\Delta\mathcal{M}_{12}\Delta\mathcal{M}_{21})\ , \tag{2.40}$$

we can write the trace log expression as

$$\frac{1}{2}\mathsf{tr}\ln\frac{\mathcal{M}}{\mathcal{M}_\infty} = \frac{1}{2}\mathsf{tr}\ln(\mathbf{1}-\Delta\mathcal{M}_{12}\Delta\mathcal{M}_{21})\ . \tag{2.41}$$

Inserting now the momentum space representation as given in Eq. (2.38), we easily evaluate the trace[8]

$$\frac{1}{2}\mathsf{tr}\ln\frac{\mathcal{M}}{\mathcal{M}_\infty} = \frac{AT_E}{(2\pi)^3}\frac{1}{2}\int_\zeta\int_{p_\parallel}\ln(1-\exp(-2Hp)) = -AT_{\mathrm{E}}\left(\frac{\pi^2}{1440H^3}\right)\ . \tag{2.42}$$

Thus we arrive again, with (2.37), at the TE-mode contribution to the force $F_{\mathrm{TE}} = -\frac{\hbar cA}{480}\frac{\pi^2}{H^4}$. By adding the TM contribution we finally find for the force density:

$$\mathcal{F}_{cas} = -\frac{\pi^2}{240}\frac{\hbar c}{H^4}\ . \tag{2.43}$$

We have seen here that the trace expression of Eq.(2.14) determining the Casimir force can be evaluated analytically for the plane surface scenario. As previously noted, for corrugated surfaces this is not the case and thus approximate methods have to be adopted.

However, as already mentioned in footnote 7 on page 10, the calculation of Casimir-Polder potentials as investigated in the following is considerable facilitated due to the fact that only one cycle of propagations has to be considered.

[8]Note that throughout this thesis the integral over momentum components $\int_p$ should be understood as $\int_{-\infty}^{\infty}\mathrm{d}p$, i.e. particularly without a factor of $\frac{1}{2\pi}$

3 Casimir-Polder forces for electromagnetic fields

In the previous section we presented a way in which Casimir forces for fluctuating scalar fields can be obtained, and accounted for a compact derivation of the famous result for the flat plate scenario. In order to tackle the atom-plate situation we now turn to a formulation that treats fluctuations of the electromagnetic field.

The outline of this section is as follows: First we will review a formalism for the calculation of fluctuation-induced forces between corrugated surfaces of materials with dielectric constants ϵ_α. We will then derive the potential energy for an atom placed in front of an ideally conducting flat plane and thus obtain the well-known result of Casimir and Polder [4].

This will be achieved by taking the dielectric constant to infinity for the first surface S_1 (i.e. make it a conductor) and expanding the dielectric constant of the second surface S_2 in terms of the atomic number density. By this process, basically S_2 is rarefied until only one atom remains.

At last we will discuss principle extensions of this formulation to the case of non-planar surfaces and discuss why this method is not well suited for such purposes.

3.1 Gauge field fluctuations and dielectric surfaces

3.1.1 Preliminaries

The formalism we review and apply here was developed in Refs. [37, 38].

The steps in the derivation of the equations for the Casimir energy and force are in principle the same as described in section 2.1.

The system's energy is found to be given in terms of the logarithm of the ratio between the restricted and unrestricted generating functionals. Inserting the proper boundary conditions into the generating functional via an appropriate δ functional allows for all functional integrals over the fields to be carried out and the expression for the Casimir energy again becomes a trace log formula as seen in section 2.

Naturally, though, the matrix entries $\mathcal{M}_{\alpha\beta}$ in the generalized case have a considerably more complicated form. First of all, here the full electromagnetic field A_μ is used instead of just scalar fields. Secondly, general dielectric materials are considered which of course also implies more involved boundary conditions for the fields.

A short review of the derivation of the trace log formula and the associated matrices $\mathcal{M}_{\alpha\beta}$ for corrugated dielectric surfaces is given in Appendix B.

3.1.2 General result for non-planar dielectric surfaces

Analogously to the previous section (cf. Eq.(2.14)), the Casimir energy in the case of zero temperature is given by

$$E_{cas}(H) = \frac{\hbar c}{T_E}\frac{1}{2}\mathsf{tr}\ln\frac{\mathcal{M}}{\mathcal{M}_\infty} \quad , \tag{3.1}$$

where $\mathcal{M}_\infty$ again stands for the propagator matrix in the case of infinite plate-plate separation.

As in the previous section, the setup should be such that the surfaces S_1 and S_2 are located at $y_3 = H_\alpha$ with $H_{1/2} = 0, H$, respectively.

However, at first we allow for deformations along the lateral coordinates $\vec{y}_\parallel = (y_1, y_2)$ which can be parametrized by height functions $h_\alpha(\vec{y}_\parallel)$.

The entries of $\mathcal{M}$ are here given by:

$$\begin{aligned}\mathcal{M}^{jl}_{\alpha\beta}(\zeta,\vec{k}_\parallel;\zeta',\vec{k}'_\parallel) = 2\pi\delta(\zeta-\zeta')\int_{\vec{y}\in S_\alpha}\int_{\vec{y}'\in S_\beta} \\ \times e^{\imath\vec{k}_\parallel\vec{y}_\parallel-\imath\vec{k}'_\parallel\vec{y}'_\parallel}e^{-[(-1)^\alpha P_\alpha(\zeta,\vec{k}_\parallel)y_3+(-1)^\beta P_\beta(\zeta',\vec{k}'_\parallel)y'_3]} \\ \times\hat{\boldsymbol{n}}_{\alpha k}\hat{\boldsymbol{n}}'_{\beta s}[\hat{\mathsf{L}}^k_\alpha(\zeta,\vec{k}_\parallel)\hat{\mathsf{L}}'^{\dagger s}_\beta(\zeta',\vec{k}'_\parallel)]_{jl}G(\zeta;\vec{y}-\vec{y}') \ .\end{aligned} \tag{3.2}$$

As before, the trace of Eq.(3.1) is to be taken over the discrete and the continuous indices. The discrete indices for this generalized setup are again the surface indices $(\alpha\ ,\ \beta)$ and the additional indices labeling the three boundary conditions $(j\ ,\ l)$ for the fluctuating fields.

The continuous variables are the frequency ζ and the momenta $\vec{k}_\parallel = (k_1, k_2)$ along the directions of two flat auxiliary surfaces R_α. For the meaning of the extra surfaces R_α, please consult Appendix B.

The spatial integrations in (3.2) are performed over the surfaces and therefore explicitly read

$$\int_{\vec{y}\in S_\alpha} = \int\sqrt{g_\alpha}\mathrm{d}y_1\mathrm{d}y_2|_{y_3=H_\alpha}, \tag{3.3}$$

with the square root of the induced surface metric

$$\sqrt{g_\alpha} = \sqrt{1+(\partial_1 h(y_\parallel))^2+(\partial_2 h(y_\parallel))^2} \ . \tag{3.4}$$

Moreover, new expressions have been defined: $P_\alpha(\zeta,\vec{k}_\parallel) \equiv \sqrt{\epsilon_\alpha(\imath\zeta)\zeta^2+\vec{k}^2_\parallel}$, with ϵ_α being the dielectric constant of the material corresponding to the respective surface S_α.

Furthermore, the normal vectors $\hat{\boldsymbol{n}}_\alpha$ with respect to the surfaces S_α are given as

$$\hat{\boldsymbol{n}}_\alpha = \frac{(-1)^\alpha}{\sqrt{g_\alpha}} \begin{pmatrix} \partial_1 h(y_\parallel) \\ \partial_2 h(y_\parallel) \\ -1 \end{pmatrix} . \tag{3.5}$$

The three operator matrices $\hat{L}^k_\alpha$ of Eq. (3.2) implement the boundary conditions on the surfaces. There, the index k labels the components of the normal vector on the surfaces S_α . The three rows essentially incorporate the three boundary conditions, whereas the four rows reflect the fact that the boundary conditions are applied to the components of the electromagnetic 4-vector potential A_μ .

The operator matrices are given as[9]:

$$\hat{\mathsf{L}}^1_\alpha(\zeta, \vec{k}_\parallel) = \begin{pmatrix} 0 & -\frac{[(-1)^\alpha P_\alpha \partial_2 + \imath k_2 \partial_3]}{\zeta \epsilon_\alpha} & \frac{[-\imath k_1 \partial_3 + (-1)^\alpha P_\alpha \partial_1]}{\zeta \epsilon_\alpha} & \frac{[\imath k_1 \partial_2 + \imath k_2 \partial_1]}{\zeta \epsilon_\alpha} \\ \imath \partial_3 & \frac{\imath k_1 \partial_3}{\zeta \epsilon_\alpha} & \frac{-\imath k_2 \partial_3}{\zeta \epsilon_\alpha} & \zeta - \frac{[\imath k_1 \partial_1 - \imath k_2 \partial_2]}{\zeta \epsilon_\alpha} \\ -\imath \partial_2 & \frac{-\imath k_1 \partial_2}{\zeta \epsilon_\alpha} & -\zeta + \frac{[(-1)^\alpha P_\alpha \partial_3 + \imath k_1 \partial_1]}{\zeta \epsilon_\alpha} & -\frac{(-1)^\alpha P_\alpha \partial_2}{\zeta \epsilon_\alpha} \end{pmatrix} \tag{3.6}$$

$$\hat{\mathsf{L}}^2_\alpha(\zeta, \vec{k}_\parallel) = \begin{pmatrix} -\imath \partial_3 & \frac{\imath k_1 \partial_3}{\zeta \epsilon_\alpha} & -\frac{\imath k_2 \partial_3}{\zeta \epsilon_\alpha} & -\zeta + \frac{[\imath k_2 \partial_2 - \imath k_1 \partial_1]}{\zeta \epsilon_\alpha} \\ 0 & \frac{[\imath k_2 \partial_3 - (-1)^\alpha P_\alpha \partial_2]}{\zeta \epsilon_\alpha} & \frac{[\imath k_1 \partial_3 + (-1)^\alpha P_\alpha \partial_1]}{\zeta \epsilon_\alpha} & -\frac{[\imath k_2 \partial_1 + \imath k_1 \partial_2]}{\zeta \epsilon_\alpha} \\ \imath \partial_1 & \zeta - \frac{[(-1)^\alpha P_\alpha \partial_3 + \imath k_2 \partial_2]}{\zeta \epsilon_\alpha} & \frac{\imath k_2 \partial_1}{\zeta \epsilon_\alpha} & \frac{(-1)^\alpha P_\alpha \partial_1}{\zeta \epsilon_\alpha} \end{pmatrix} \tag{3.7}$$

$$\hat{\mathsf{L}}^3_\alpha(\zeta, \vec{k}_\parallel) = \begin{pmatrix} \imath \partial_2 & \frac{-\imath k_1 \partial_2}{\zeta \epsilon_\alpha} & \zeta + \frac{[\imath k_1 \partial_1 + (-1)^\alpha P_\alpha \partial_3]}{\zeta \epsilon_\alpha} & -\frac{(-1)^\alpha P_\alpha \partial_2}{\zeta \epsilon_\alpha} \\ -\imath \partial_1 & -\zeta - \frac{[\imath k_2 \partial_2 + (-1)^\alpha P_\alpha \partial_3]}{\zeta \epsilon_\alpha} & \frac{\imath k_2 \partial_1}{\zeta \epsilon_\alpha} & \frac{(-1)^\alpha P_\alpha \partial_1}{\zeta \epsilon_\alpha} \\ 0 & \frac{[(-1)^\alpha P_\alpha \partial_2 - \imath k_2 \partial_3]}{\zeta \epsilon_\alpha} & \frac{[\imath k_1 \partial_3 - (-1)^\alpha P_\alpha \partial_1]}{\zeta \epsilon_\alpha} & \frac{[\imath k_2 \partial_1 - \imath k_1 \partial_2]}{\zeta \epsilon_\alpha} \end{pmatrix} \tag{3.8}$$

[9]It should be noted that the matrices of Eqs. (3.6-3.8) are obtained from their pendants in Appendix B (cf. Eqs. (B.11-B.13)) through the substitutions $(\bar{\partial}_1, \bar{\partial}_2) \to -\imath(k_1, k_2)$ and $\bar{\partial}_3 \to (-1)^\alpha P_\alpha$.

and their corresponding adjoint matrices of the primed coordinates.

The Green's function G in (3.2) is the free photon propagator in Feynman gauge; its representation in momentum space reads

$$G(\zeta, \vec{k}) = (\zeta^2 + \vec{k}^2)^{-1} \ . \tag{3.9}$$

In the following a representation of the Green's function will be useful where only the third component of the function is transformed to position space. Making use of the residue formula upon integration, it can be obtained from (3.9) and yields

$$G(\zeta; \vec{k}_\parallel, x_3) = \frac{e^{-P(\zeta,\vec{k}_\parallel)|x_3|}}{2P(\zeta, \vec{k}_\parallel)} \ , \tag{3.10}$$

with the abbreviation

$$P(\zeta, \vec{k}_\parallel) = \sqrt{\zeta^2 + \vec{k}_\parallel^2} \ . \tag{3.11}$$

3.2 Casimir-Polder result through thinning of one plate

3.2.1 The limit of flat surfaces

In the limit of flat surfaces, the general expression of Eq. (3.2) can be simplified considerably.

As in section 2.2, we choose our setup such that the two surfaces S_α are located at $y_3 = H_\alpha$, where $H_1 = 0$ and $H_2 = H$.

Again, the problem is translationally invariant along the lateral coordinates and the time direction and therefore it is convenient to work in momentum space with respect to those coordinates.

Also for planar surfaces it holds that their normal vector takes a very simple form. For the two plates in our setup we find with the definition (3.5) that $\hat{\boldsymbol{n}}_1 = (0, 0, 1)$ and $\hat{\boldsymbol{n}}_2 = (0, 0, -1)$ since the height functions vanish.

Therefore in this setup, only the last matrix as given in Eq.(3.8) is of relevance.

We now make use of the partially transformed photon propagator as given in Eq.(3.10). Applying the representation of the Green's function

$$G(\zeta; \vec{y} - \vec{y}') \ = \int \frac{\mathrm{d}q_\parallel}{(2\pi)^2} \frac{e^{-P(\zeta,\vec{q}_\parallel)|y_3 - y_3'|}}{2P(\zeta, \vec{q}_\parallel)} \ e^{-\imath \vec{q}_\parallel \vec{y}_\parallel} \ , \tag{3.12}$$

in Eq. (3.2), we can execute the partial derivatives ∂_1,∂_2 appearing in the operator matrix (3.8) yielding $\partial_1 \to -\imath q_1$ and $\partial_2 \to -\imath q_2$. Thereafter the integrals over $\vec{y}_\parallel$, $\vec{y}'_\parallel$ and $\vec{q}_\parallel$ can be carried out implying $\partial_1 \to -\imath k_1$ and $\partial_2 \to -\imath k_2$.

Equation (3.2) now acquires a very simple form:

$$\mathcal{M}_{\alpha\beta}(\zeta,\vec{k}_\parallel;\zeta',\vec{k}'_\parallel) = (2\pi)^3\delta(\zeta-\zeta')\delta^{(2)}(\vec{k}_\parallel-\vec{k}'_\parallel)\eta_{\alpha\beta} \times[\hat{\mathsf{L}}^3_\alpha(\zeta,\vec{k}_\parallel)\hat{\mathsf{L}}'^{\dagger 3}_\beta(\zeta',\vec{k}'_\parallel)]_{jl}\frac{e^{-P(\zeta,\vec{k}_\parallel)|y_3-y'_3|}}{2P(\zeta,\vec{k}_\parallel)}\bigg|_{y_3=H_\alpha,y'_3=H_\beta} . \quad (3.13)$$

The factor $\eta_{\alpha\beta} \equiv (-1)^{\alpha+\beta}e^{-[(-1)^\alpha P_\alpha(\zeta,\vec{k}_\parallel)H_\alpha+(-1)^\beta P_\beta(\zeta',\vec{k}'_\parallel)H_\beta]}$ will drop out in the calculation of the Casimir-Polder potential as we will show at the end of this section and we will therefore omit this factor temporarily.

3.2.2 Plane metallic and plane dielectric surface

We now want to choose S_1 as an ideal conductor and therefore let $\epsilon_1 \to \infty$. S_2 shall remain a general dielectric since this is the side where the atom will be located.

First, we want to write down the explicit form of the remaining operator matrices for the surfaces, respectively. Equation (3.8) in the limit of a diverging dielectric function ϵ_1 of the material bounded by S_1 reduces to

$$\hat{\mathsf{L}}^3_1(\zeta,\vec{k}_\parallel) = \begin{pmatrix} k_2 & 0 & \zeta & 0 \\ -k_1 & -\zeta & 0 & 0 \\ 0 & 0 & 0 & 0 \end{pmatrix} , \quad (3.14)$$

whilst the matrix for the surface S_2 is obtained from (3.8) through the substitutions $(\partial_1,\partial_2) \to (-\imath k_1,-\imath k_2)$:

$$\hat{\mathsf{L}}^3_2(\zeta,\vec{k}_\parallel) = \begin{pmatrix} k_2 & -\frac{k_1k_2}{\zeta\epsilon_2} & \zeta+\frac{1}{\zeta\epsilon_2}[k_1^2+P_2\partial_3] & \frac{\imath k_2P_2}{\zeta\epsilon_2} \\ -k_1 & -\zeta-\frac{1}{\zeta\epsilon_2}[k_2^2+P_2\partial_3] & \frac{k_1k_2}{\zeta\epsilon_2} & -\frac{\imath k_1P_2}{\zeta\epsilon_2} \\ 0 & -\frac{\imath k_2}{\zeta\epsilon_2}[P_2+\partial_3] & \frac{\imath k_1}{\zeta\epsilon_2}[P_2+\partial_3] & 0 \end{pmatrix} . \quad (3.15)$$

Next we note, that in (3.15) the third row is in fact linearly dependent on the first two rows, because for the rows $\hat{\mathsf{L}}^3_{2,i}$ it holds that $-\imath p_2\hat{\mathsf{L}}^3_{2,3\mu} = k_1\hat{\mathsf{L}}^3_{2,1\mu}+k_2\hat{\mathsf{L}}^3_{2,2\mu}$, where μ numbers the columns.

This is expected since for flat surfaces only two boundary conditions for the electric field remain independent and the problem can again be formulated in terms of one transversal electric and one transversal magnetic field component (cf. [37], Appendix A). We can therefore work in the subspace of linearly independent entries.

By applying the last remaining derivatives ∂_3 and ∂'_3 in (3.15) onto the Green's function of Eq.(3.13)

$$G(\zeta;\vec{k}_\parallel,x_3)=\frac{e^{-P(\zeta,\vec{k}_\parallel)|y_3-y'_3|}}{2P(\zeta,\vec{k}_\parallel)}\ , \tag{3.16}$$

and evaluating the 3-component on the respective surfaces, we obtain all propagator matrices $\mathcal{M}_{\alpha\beta}$. Since they are all diagonal in their momenta, the inversion of the propagators $\mathcal{M}_{22}$ and $\mathcal{M}_{11}$ is an easy task.

As we know from section 2.2, the expansion of the logarithm in the formula for the Casimir energy leads to an expression that demands the evaluation of the traces of propagation cycles. Following the same steps as in the derivation for scalar fields, we find that the energy (3.1) between the dielectric (D) and the metal (M) plate is given by

$$E_{DM}=-\sum_{n=1}^{\infty}\frac{1}{2n}\frac{\hbar c}{T_E}\mathsf{tr}[(\mathcal{M}_{11}^{-1}\mathcal{M}_{12}\mathcal{M}_{22}^{-1}\mathcal{M}_{21})^n]\ . \tag{3.17}$$

From here on we omit the factors of $(2\pi)^3\delta(\zeta-\zeta')\delta^{(2)}(\vec{k}_\parallel-\vec{k}'_\parallel)$ in Eq.(3.13), since the factors of $(2\pi)^3$ appear twice in the nominator and twice in the denominator in (3.17) and therefore cancel; the distributions $\delta(\zeta-\zeta')$ and $\delta^{(2)}(\vec{k}_\parallel-\vec{k}'_\parallel)$ just kill the integrals over the primed variables and from here on we set $\zeta=\zeta'$ and $\vec{k}_\parallel=\vec{k}'_\parallel$.

The associated inverse propagators on the surfaces and the propagator between the surfaces now read explicitly:

$$\mathcal{M}_{11}^{-1}(\zeta,\vec{k}_\parallel) = \frac{2}{\zeta^2 P}\begin{pmatrix} k_1^2+\zeta^2 & k_1k_2 \\ k_1k_2 & k_2^2+\zeta^2\end{pmatrix} \tag{3.18}$$

$$\begin{aligned}\mathcal{M}_{12}(\zeta,\vec{k}_\parallel) &= \frac{1}{2P}e^{-PH} \\ &\times\begin{pmatrix} k_2^2+\zeta^2+\frac{1}{\epsilon_2}[k_1^2-PP_2] & -\left(\frac{\epsilon_2-1}{\epsilon_2}\right)k_1k_2 \\ -\left(\frac{\epsilon_2-1}{\epsilon_2}\right)k_1k_2 & k_1^2+\zeta^2+\frac{1}{\epsilon_2}[k_2^2-PP_2]\end{pmatrix}\end{aligned} \tag{3.19}$$

$$\begin{aligned}\mathcal{M}_{22}^{-1}(\zeta,\vec{k}_\parallel) &= \frac{2P\epsilon_2^2}{\left[(\epsilon_2-1)P_2((1+\epsilon_2)\vec{k}_\parallel^2+\epsilon_2\zeta^2)\right]} \\ &\times\begin{pmatrix}(1+\epsilon_2)k_1^2+k_2^2+\epsilon_2\zeta^2 & \epsilon_2k_1k_2 \\ \epsilon_2k_1k_2 & (1+\epsilon_2)k_2^2+k_1^2+\epsilon_2\zeta^2\end{pmatrix}\ ,\end{aligned} \tag{3.20}$$

with $\mathcal{M}_{21}(\zeta,\vec{k}_\parallel)=\mathcal{M}_{12}(\zeta,\vec{k}_\parallel)$ as the setup obviously is symmetric.

It should be mentioned that the propagators (3.18-3.20) together with the log det formula for the Casimir free energy (cf. Eq. (B.24) in Appendix B) yield the Lifshitz formula for the interaction energy between a plane metallic and a plane dielectric surface [5, 39]. This is shown in [37] for the general case of two planar dielectrics.

3.2.3 Making an atom out of the dielectric surface

Now we will argue that considering only the first series term in Eq. (3.17) suffices to obtain the exact Casimir-Polder result.

In order to calculate the energy of just one atom near the metal wall, we expand the dielectric permittivity ϵ_2 corresponding to the surface S_2 in terms of the number of atoms per unit volume and preserve only the contribution of first order, since the higher-order contributions account for the atom-atom interaction inside the dielectric [39, 40].

The dielectric constant of S_2 hence is expanded as

$$\epsilon_2 = 1 + a(\imath\zeta)N + \mathcal{O}(N^2)\ , \tag{3.21}$$

where we have set $a(\imath\zeta)=4\pi\chi(\imath\zeta)$ with $\chi(\imath\zeta)$ being the dynamical polarizability of just one atom.

Upon expansion in N we find for the propagators of Eqs. (3.18-3.20) on and in between the two plates the following expressions[10]:

$$\mathcal{M}_{11}^{-1}(\zeta,\vec{k}_\parallel) = \frac{2}{\zeta^2 P}\begin{pmatrix} k_1^2+\zeta^2 & k_1k_2 \\ k_1k_2 & k_2^2+\zeta^2 \end{pmatrix} \tag{3.22}$$

$$\mathcal{M}_{12}(\zeta,\vec{k}_\parallel) = \frac{a(\imath\zeta)Ne^{-2PH}}{2P}\begin{pmatrix} k_2^2+\frac{\zeta^2}{2} & -k_1k_2 \\ -k_1k_2 & k_1^2+\frac{\zeta^2}{2} \end{pmatrix} + \mathcal{O}(N^2) \tag{3.23}$$

$$\mathcal{M}_{22}^{-1}(\zeta,\vec{k}_\parallel) = \frac{2}{a(\imath\zeta)NP}\frac{1}{(2k_1^2+2k_2^2+\zeta^2)} \begin{pmatrix} 2k_1^2+k_2^2+\zeta^2 & k_1k_2 \\ k_1k_2 & k_1^2+2k_2^2+\zeta^2 \end{pmatrix} + \mathcal{O}(1)\ . \tag{3.24}$$

As we see, the product $\mathcal{M}_{11}^{-1}\mathcal{M}_{12}\mathcal{M}_{22}^{-1}\mathcal{M}_{21}$ already is of order N.

[10] The inverse propagator on the metal plane $\mathcal{M}_{11}^{-1}$ of course does not contain ϵ_2. We just repeat it in order to have all the relevant matrices in one place.

Thus, only the first cycle of fluctuations contributes and with Eq.(3.17) the energy density between the rarefied dielectric and the metal can be written as

$$\mathcal{E}_{DM} = -\frac{1}{2}\frac{\hbar c}{AT_E}\mathsf{tr}(\mathcal{M}_{11}^{-1}\mathcal{M}_{12}\mathcal{M}_{22}^{-1}\mathcal{M}_{21}) + \mathcal{O}(N^2) \ , \tag{3.25}$$

where higher order traces are irrelevant for the Casimir-Polder limit.

Using the propagators as given in Eqs.(3.22-3.24), we find that Eq.(3.25) becomes

$$\mathcal{E}_{DM} = -\frac{\hbar c}{2}\frac{1}{(2\pi)^3}\int_\zeta\int_{\vec{k}_\parallel}\frac{a(\imath\zeta)N}{2}e^{-2H\sqrt{\zeta^2+\vec{k}_\parallel}} + \mathcal{O}(N^2) \ . \tag{3.26}$$

One can now put in the definition $a(\imath\zeta) = 4\pi\chi(\imath\zeta)$, and evaluate the integrations over the lateral momenta $\vec{k}_\parallel$.

The energy density then reads

$$\mathcal{E}_{DM} = -N\frac{\hbar c}{8\pi H}\int_0^\infty \mathrm{d}\zeta(1+2H\zeta)e^{-2H\zeta}\chi(\imath\zeta) \ + \mathcal{O}(N^2) \ . \tag{3.27}$$

In the limit of large separations, the dominant frequencies correspond to a wavelength of order H. Hence, only the static polarizability is relevant and one can approximate $\chi(\imath\zeta) \approx \chi(0)$. The integration over the frequency can then be performed and yields

$$\mathcal{E}_{DM} = -N\chi(0)\frac{\hbar c}{8\pi H^3} + \mathcal{O}(N^2) \ . \tag{3.28}$$

The energy of this dilute dielectric in front of a metal plane can be viewed as being composed out of the required energy for bringing N atoms from distance H to infinity. Therefore, the energy of one atom in front of a metal wall is obtained by solving

$$\mathcal{E}_{DM}(H) = N\int_H^\infty E_{AM}(y_3)dy_3 + \mathcal{O}(N^2) \tag{3.29}$$

for E_{AM} and taking the limit $N \to 0$.

Thus we get the well-known formula first derived by Casimir and Polder in Ref. [4]:

$$E_{AM}(H) = -\frac{3\hbar c}{8\pi H^4}\chi(0) \ . \tag{3.30}$$

It accounts for the potential energy of the atom-plate configuration in the retarded limit.

At last, we come back to the omitted factor of $\eta_{\alpha\beta}$ introduced below Eq.(3.13).

In the matrix product of $\mathcal{M}_{11}^{-1}\mathcal{M}_{12}\mathcal{M}_{22}^{-1}\mathcal{M}_{21}$ appearing in Eq. (3.25) it contributes with a factor of $(1)\cdot(-e^{-P_2H})\cdot(-e^{-P_2H})\cdot(e^{2P_2H}) = 1$ and therefore ignoring $\eta_{\alpha\beta}$ was justified in our calculation.

3.3 Extension to corrugated surfaces

As elaborated in section 3.1.2, the formulation of the theory for dielectric surfaces from the outset is valid for biaxially corrugated surfaces whose deformations along the lateral coordinates can be parametrized by height functions $h(\vec{y}_\parallel)$. Therefore a transfer of the thinning technique as used in the previous section onto structured surfaces seems to bear no principle obstruction, though the calculations become of course considerably more involved: The introduction of non-planar surfaces renders the matrices of Eq. (3.2) non-diagonal and makes their inversion a cumbersome task.

Although the method of expanding the dielectric constant in terms of the atomic number density provides a very intuitive access to a Casimir-Polder setup, it has its flaws in the context of nontrivially shaped surfaces.

Roughly spoken, the translational invariance of the dielectric plate which is thinned out also passes into a translational invariance of the atom with respect to the plate. This is fine in the case of planar surfaces, but poses a problem for the case of corrugated surfaces since translational invariance in the spatial components is not given anymore when the metallic plate is structured.

Therefore, by the thinning of the dielectric surface one looses the information of where exactly the atom is located along the line of corrugation and cannot extract the desired potential function. Considering e.g. a surface uniaxially structured along the direction x_1, this means that one cannot obtain the local information $V(x_1, H)$ but only an average potential which is integrated over the variable x_1.

A possible way out of this dilemma would be to work with a formulation allowing for a spatially dependent dielectric function $\epsilon_2(x_1)$ in order to break the translational invariance along S_2. However, this choice disproportionately complicates the formulation, since already the determination of the Green's function inside the material is a nontrivial task (cf. Eq.(B.8)).

We therefore seek a different way of calculating the Casimir-Polder potential for arbitrarily structured surfaces. In the following, instead of the thinning process, we will approximate the atom as a sphere located at *defined* lateral coordinates above the surface.

We will see that this setup overcomes the deficiency of the thinning method as described above and perfectly allows for the local information of the potential to be extracted.

4 Scalar Casimir-Polder potential for planar surfaces

What we want to elaborate on here is a calculation of the Casimir potential for a massless scalar field between a Dirichlet sphere and a flat plate. The plate - as in the previous sections - should be considered as infinitely extended along the directions x_1 and x_2.

We label the plate as surface S_1 positioned at $x_3 = 0$ and the sphere as surface S_2 with the centre of the sphere being located at $x_3 = H$. Let the radius of the sphere be r. See Figure 1.

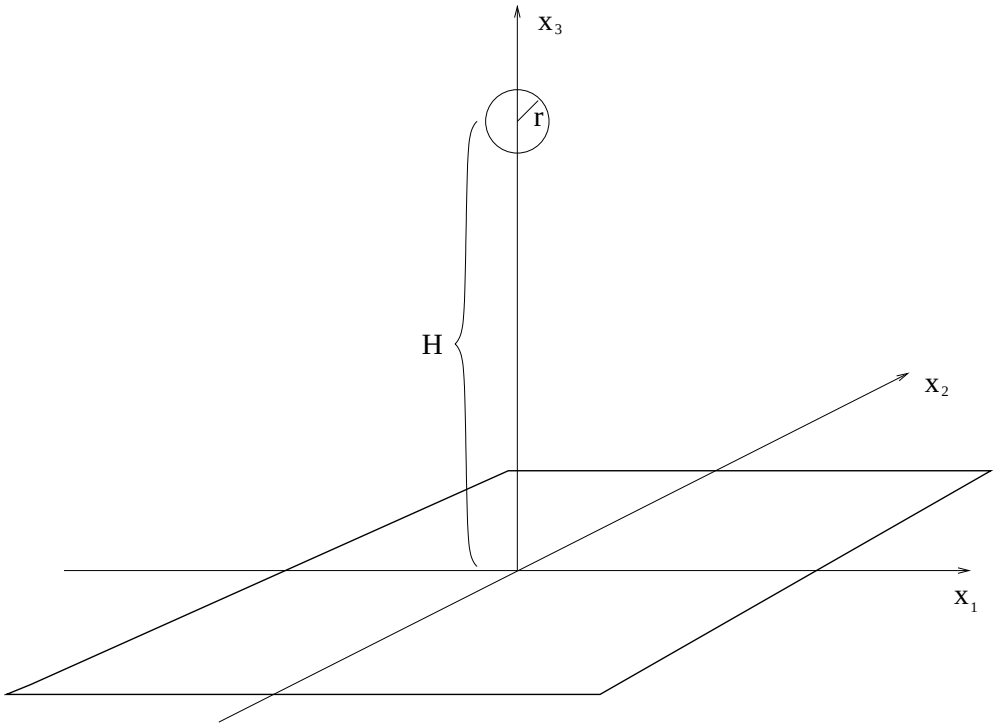

Figure 1: A sphere of radius r is placed atop a planar surface. The mean distance between the surface and the sphere be H.

The outline of this section is as follows:

First of all, we will give explicit representations of the relevant propagators $\mathcal{M}_{\alpha\beta}$ for this setup. We will then derive the Casimir potential for a flat surface-sphere configuration up to $\mathcal{O}\left(\frac{r}{H^2}\right)$ in the Casimir-Polder limit $\frac{r}{H} \ll 1$. This calculation will be performed in position space with respect to the spatial components since translational invariance in all spatial directions is broken by the introduction of the sphere.

Considering the trace expression for the Casimir energy and force (cf. (2.24)), this implies that we start from an outset of nine integrations: one integration over the frequency, since the matrices are still diagonal in the time component, and four times two integrations over the spatial components of the two-dimensional surfaces.

However, as we perform the calculation we will find that in the desired approximation all angular integrations over the sphere become trivial. This will then allow us to deduce a notably simplified formula for the Casimir-Polder potential which only demands the integrations over the frequency and the coordinates on the plane.

Furthermore, similar to the previous section, we will see that in the order $\mathcal{O}\left(\frac{r}{H^2}\right)$ only the first expansion term of the logarithm of the trace log formula contributes to the energy in the Casimir-Polder potential.

These two properties, namely the vanishing of the atom-side integrals and the negligibility of higher order trace terms will then be of great use when nontrivial geometries are considered and allow for a compact and efficient numerical computation of the potentials for corrugated surfaces (see section 5).

4.1 Propagators in the sphere-plane setup

At first we want to introduce the propagators on and between the surfaces as needed for the computation of the potential.

Consider again the Green's function of this problem for four-vectors x, x' as presented in the previous section (cf. Eq. (2.9)):

$$G(x, x') = \frac{1}{4\pi^2} \frac{1}{(x - x')^2} \tag{4.1}$$

The functional inversion of this propagator for coordinates x,x' on a flat plate is an easy task because of its diagonality in momentum space. Clearly this property is lost with respect to the spatial components of the four-vectors when x and x' are evaluated on the sphere. We will therefore at first only Fourier transform the time-like component of the propagators to frequency space, i.e. we calculate

$$\mathcal{M}_{\alpha\beta}(\zeta, \vec{x} - \vec{x}') = \int_{\tilde{x}_0} \mathcal{M}_{\alpha\beta}(\tilde{x}_0, \vec{x} - \vec{x}') e^{\imath\zeta\tilde{x}_0} \ , \tag{4.2}$$

where $\tilde{x}_0$ is shorthand for the difference of the time components $\tilde{x}_0 = x_0 - x_0'$.

For calculational convenience we choose a proper time representation such that the spatial dependence factorizes.

The matrix elements of $\mathcal{M}$ then read:

$$\mathcal{M}_{\alpha\beta}(\zeta, \vec{x} - \vec{x}') = \int_0^\infty dT \frac{1}{\sqrt{4\pi T}} \times \exp\left(-4\pi^2(\vec{x} - \vec{x}')^2 T\right) \exp\left(-\frac{\zeta^2}{16\pi^2 T}\right) , \quad (4.3)$$

with $\vec{x} = (x_1, x_2, x_3)$.

As in the flat plate scenario we will need all propagators on and in between the surfaces. Let us first consider the inverse propagator on the sphere.

4.1.1 Inverse propagator on a sphere

With the representation of Eq.(4.3), the inverse of $\mathcal{M}_{22}$ can be determined by solving

$$\int_{\vec{x}' \in S_2} \mathcal{M}_{22}^{-1}(\zeta, \vec{x}, \vec{x}') \mathcal{M}_{22}(\zeta, \vec{x}', \vec{x}'') = \delta^{(3)}(\vec{x} - \vec{x}'')\big|_{\vec{x}, \vec{x}'' \in S_2} , \quad (4.4)$$

where the spatial integration is performed over the surface of the sphere S_2.

In order to solve this equation for $\mathcal{M}_{22}^{-1}$ we first rewrite Eq. (4.4) in polar coordinates:

$$r^2 \int_{\Omega'} \mathcal{M}_{22}^{-1}(\zeta, \Omega, \Omega') \mathcal{M}_{22}(\zeta, \Omega', \Omega'') = \frac{1}{r^2} \delta(\phi - \phi'') \delta(\cos\theta - \cos\theta'') , \quad (4.5)$$

with the usual definition $\int_{\Omega'} = \int_0^{2\pi} \mathrm{d}\phi' \int_{-1}^{1} \mathrm{d}(\cos\theta')$.

We now see that the dynamical variables of the propagator are just the polar and the azimuthal angles and thus $\mathcal{M}_{22}(\zeta, \Omega', \Omega'')$ as well as $\mathcal{M}_{22}^{-1}(\zeta, \Omega, \Omega')$ can be expanded in terms of spherical harmonics:

$$\mathcal{M}_{22}(\zeta, \Omega', \Omega'') = \sum_{l=0}^{\infty} \sum_{m=-l}^{l} c_l(\zeta) Y_{lm}(\Omega') Y_{lm}^\star(\Omega'') \quad (4.6)$$

$$\mathcal{M}_{22}^{-1}(\zeta, \Omega, \Omega') = \sum_{l'=0}^{\infty} \sum_{m'=-l'}^{l'} b_{l'}(\zeta) Y_{l'm'}(\Omega) Y_{l'm'}^\star(\Omega') \quad (4.7)$$

with the expansion coefficients c_l, b_l of $\mathcal{M}_{22}$ and $\mathcal{M}_{22}^{-1}$, respectively.

On the right hand side of the determining equation (4.5) we can insert the representation of the δ functions in terms of spherical harmonics.

Equation (4.4) then reads

$$\int_{\Omega'} \sum_{l'=0}^{\infty} \sum_{m'=-l'}^{l'} \sum_{l=0}^{\infty} \sum_{m=-l}^{l} b_{l'}(\zeta) Y_{l'm'}(\Omega) Y^{\star}_{l'm'}(\Omega') c_l(\zeta) Y_{lm}(\Omega') Y^{\star}_{lm}(\Omega'') = \frac{1}{r^4} \sum_{l=0}^{\infty} \sum_{m=-l}^{l} Y_{lm}(\Omega) Y^{\star}_{lm}(\Omega'') \ . \quad (4.8)$$

Subsequently, making use of the completeness relation for spherical harmonics

$$\int_{\Omega'} Y^{\star}_{l'm'}(\Omega') Y_{lm}(\Omega') = \delta_{l'l} \delta_{m'm} \ , \quad (4.9)$$

the expansion coefficients of $\mathcal{M}_{22}^{-1}$ can be determined to arbitrary order by comparison of coefficients. For the expansion coefficients of the inverse propagator it holds that

$$b_l(\zeta) = \frac{1}{r^4} \frac{1}{c_l(\zeta)} \ . \quad (4.10)$$

In order to determine the coefficients $c_l(\zeta)$, we write the propagator $\mathcal{M}_{22}$ of Eq.(4.3) as

$$\mathcal{M}_{22}(\zeta, \Omega', \Omega'') = \int_0^{\infty} dT \frac{1}{\sqrt{4\pi T}} \exp\left[-\frac{\zeta^2}{16\pi^2 T}\right] \times \exp\left[-8\pi^2 r^2 T \left(1 - \cos\alpha\right)\right] \quad (4.11)$$

where α is the angle between the vectors $\vec{x}'$ and $\vec{x}''$ and thus $\cos\alpha$ is defined as $\cos\alpha = \sin\theta' \sin\theta'' \cos(\phi' - \phi'') + \cos\theta' \cos\theta''$.

We see now the advantage of the proper time representation: The angular contribution factorizes and the exponential function in Eq. (4.11) carrying the angular part can be expanded in terms of Legendre polynomials $P_l(\cos\alpha)$:

$$\exp\left[-8\pi^2 r^2 T \left(1 - \cos\alpha\right)\right] = \sum_{l=0}^{\infty} \tilde{c}_l P_l(\cos\alpha) \ , \quad (4.12)$$

where $\tilde{c}_l = \frac{2l+1}{2} \int_0^{\pi} \mathrm{d}\alpha \exp\left[-8\pi^2 r^2 T \left(1 - \cos\alpha\right)\right] P_l(\cos\alpha) \sin(\alpha)$.

Making use of the addition theorem for the spherical harmonics

$$P_l(\cos\alpha) = \frac{4\pi}{2l+1} \sum_{m=-l}^{l} Y^{\star}_{lm}(\Omega') Y_{lm}(\Omega'') \ , \quad (4.13)$$

we finally find that the expansion coefficients $c_l(\zeta)$ of the propagator on the sphere are given by

$$c_l(\zeta) = \int_0^\infty \mathrm{d}T \sqrt{\frac{\pi}{T}} \exp\left(-\frac{\zeta^2}{16\pi^2 T}\right) \times \int_0^\pi \mathrm{d}\alpha \exp\left[-8\pi^2 r^2 T(1-\cos(\alpha))\right] P_l(\cos\alpha)\sin(\alpha) \ . \quad (4.14)$$

Thus, using the relation (4.10), one finds that Eq. (4.7) reads up to dipole order:

$$\mathcal{M}_{22}^{-1}(\zeta,\phi,\theta;\phi',\theta') = \frac{1}{4\pi}\frac{|\zeta|\exp(r|\zeta|)}{r^2\sinh(r|\zeta|)} + \frac{3}{2\pi}\frac{\exp(2r|\zeta|)|\zeta|^5\left[\cos\theta\cos\theta' + \imath\sin\theta\sin\theta'\sin(\phi-\phi')\right]}{\zeta^2\left(1+r^2\zeta^2+\exp(2r|\zeta|)[\zeta^2r^2-1]+2r|\zeta|\right)} \ . \quad (4.15)$$

In the limit of $\frac{r}{H} \to 0$, the dominant contribution is determined by the monopole order. We will therefore restrict ourselves to the first term in (4.15) and work with

$$\mathcal{M}_{22}^{-1}(\zeta) = \frac{1}{4\pi}\frac{|\zeta|\exp(r|\zeta|)}{r^2\sinh(r|\zeta|)} \ . \quad (4.16)$$

Note, that $\mathcal{M}_{22}^{-1}$ in this approximation is independent of the angles Ω, Ω' as we are considering monopole order.

4.1.2 Propagators between sphere and surface

As far as the other propagators are concerned, we now benefit from the expressions which were already derived in the context of two flat plates in section 2.2.2. Rewriting our result for the combination of a propagation on a flat surface with the propagation to a surface at distance H (cf. Eq. (2.30)), we get $\Delta\mathcal{M}_{12}$ for the sphere-plane setup.

We use it again in a proper time representation:

$$\Delta\mathcal{M}_{12}(\zeta,\vec{x}_\parallel;\Omega) = \frac{1}{\pi^{\frac{3}{2}}}(H+r\cos\theta)\int_0^\infty dS\sqrt{S}\exp\left(-\frac{\zeta^2}{4S}\right) \times \exp\left(-\left[(x_1-r\cos\phi\sin\theta)^2+(x_2-r\sin\phi\sin\theta)^2+(H+r\cos\theta)^2\right]S\right) \ , \quad (4.17)$$

where the vector pointing onto the surface is given in terms of polar coordinates.

The missing ingredient for a full cycle of propagations is $\mathcal{M}_{21}$ which is determined through Eq.(4.3) as presented in the beginning of this section.

It reads

$$\mathcal{M}_{21}(\zeta,\Omega;\vec{x}_\parallel) = \int_0^\infty dT \frac{1}{\sqrt{4\pi T}} \exp\left(-\frac{\zeta^2}{16\pi^2 T}\right) \exp\left(-4\pi^2\left[(r\cos\phi\sin\theta - x_1)^2 + (r\sin\phi\sin\theta - x_2)^2 + (H + r\cos\theta)^2\right]T\right) . \tag{4.18}$$

With the associated propagators of Eqs. (4.16-4.18) at hand we can now calculate the potential energy of the sphere-plane configuration.

4.2 Potential energy in the sphere-plane setup

4.2.1 Exact energy in the Casimir-Polder limit

As argued in section 2.2, the value of the Casimir energy is essentially determined by the trace over a cycle of fluctuation propagations:

$$\mathsf{tr}\left[\left(\mathcal{M}_{11}^{-1}\mathcal{M}_{12}\mathcal{M}_{22}^{-1}\mathcal{M}_{21}\right)^n\right] = \mathsf{tr}\left[\left(\Delta\mathcal{M}_{12}\mathcal{M}_{22}^{-1}\mathcal{M}_{21}\right)^n\right] \tag{4.19}$$

with n indicating the number of cycles. For a potential of $\mathcal{O}\left(\frac{r}{H^2}\right)$ though, we will see in a moment that one cycle suffices, i.e. traces of order $n > 1$ are not needed in this limit.

As a side remark we note that in this setup it is not only convenient to work with the combined propagator $\Delta\mathcal{M}_{12} = \mathcal{M}_{11}^{-1}\mathcal{M}_{12}$ as indicated in Eq. (4.19) but also highly advisable. Trying to perform the inner integrations over the surfaces in $\mathcal{M}_{11}^{-1}\mathcal{M}_{12}\mathcal{M}_{22}^{-1}\mathcal{M}_{21}$ in any other order significantly complicates the remaining integrals and makes them substantially harder to evaluate.

Now, with the expressions for the propagators known from the previous subsection, we can write out the trace for the flat surface - sphere configuration with its explicit dependencies on the frequency ζ, the angular variables Ω on the sphere, and the lateral coordinates $\vec{x}_\parallel$ on the plate:

$$\mathsf{tr}\left(\Delta\mathcal{M}_{12}\mathcal{M}_{22}^{-1}\mathcal{M}_{21}\right) = \frac{T_E}{2\pi}\int_\zeta\int_{\vec{x}_\parallel}\int_\Omega\int_{\Omega'} r^4\Delta\mathcal{M}_{12}(\zeta,\vec{x}_\parallel;\Omega)\mathcal{M}_{22}^{-1}(\zeta)\mathcal{M}_{21}(\zeta,\Omega';\vec{x}_\parallel) . \tag{4.20}$$

As mentioned in the outline of this section, the propagators of Eq.(4.20) do not depend on the solid angle in the desired approximation and therefore the angular integrations over the sphere become trivial.

To see this, we first rescale the dimensionful integration variables of Eq. (4.20) with H, such that all integration parameters become dimensionless.

We do this in order to extract the dimensionful dependency of the trace and thereby deduct a formula that points out the physical scaling of the energy within this configuration. The factor that contains just dimensionless quantities is separated and provides only for the numerical factor of the scaling.

In particular this means that we rewrite the lateral coordinates and the imaginary frequency through $\vec{x}_\parallel \to \tilde{\vec{x}}_\parallel H$ and $\zeta \to \frac{\tilde{\zeta}}{H}$ with new dimensionless tilded variables. Additionally one should not forget to rescale also the dimensionful auxiliary integration variables in the proper time representations of $\Delta\mathcal{M}_{12}$ and $\mathcal{M}_{21}$ via the substitutions $S \to \frac{\tilde{S}}{H^2}$ and $T \to \frac{\tilde{T}}{H^2}$.

To see that the auxiliary integration variables T and S bear a spatial dimension of $[-2]$ please refer to Eqs.(4.17) and (4.18). There, the exponential carrying the spatial dependencies becomes dimensionless if T as well as S are of dimension $[-2]$.

Again we initially consider the properties of the propagator on the sphere.

After rescaling, Eq. (4.16) reads

$$\mathcal{M}_{22}^{-1}(\tilde{\zeta}) = \frac{1}{4\pi}\frac{\frac{|\tilde{\zeta}|}{H}\exp(\frac{r}{H}|\tilde{\zeta}|)}{r^2\sinh(\frac{r}{H}|\tilde{\zeta}|)} \ . \tag{4.21}$$

Assuming the limit of $\frac{r}{H} \ll 1$ we see that the hyperbolic sine in (4.21) can be approximated by its argument while the exponential is approximated by 1, i.e. we have

$$\mathcal{M}_{22}^{-1}(\tilde{\zeta}) = \frac{1}{4\pi}\frac{1}{r^3} + \mathcal{O}\left(\frac{r}{H}|\tilde{\zeta}|\right) \ . \tag{4.22}$$

Furthermore upon rescaling, Eqs. (4.17) and (4.18) now read:

$$\Delta\mathcal{M}_{12}(\tilde{\zeta},\tilde{\vec{x}}_\parallel;\Omega) = \frac{1}{\pi^{\frac{3}{2}}}(1+\frac{r}{H}\cos\theta)\int_0^\infty d\tilde{S}\sqrt{\tilde{S}}\exp\left(-\frac{\tilde{\zeta}^2}{4\tilde{S}}\right)$$
$$\times\exp\left(-\left[(\tilde{x}_1-\frac{r}{H}\cos\phi\sin\theta)^2+(\tilde{x}_2-\frac{r}{H}\sin\phi\sin\theta)^2+(1+\frac{r}{H}\cos\theta)^2\right]\tilde{S}\right) \ , \tag{4.23}$$

and

$$\mathcal{M}_{21}(\tilde{\zeta},\Omega';\tilde{\vec{x}}_\parallel) = \int_0^\infty d\tilde{T}\frac{1}{\sqrt{4\pi\tilde{T}}}\exp\left(-\frac{\tilde{\zeta}^2}{16\pi^2\tilde{T}}\right)$$
$$\times\exp\left(-4\pi^2\left[(\frac{r}{H}\cos\phi'\sin\theta'-\tilde{x}_1)^2+(\frac{r}{H}\sin\phi'\sin\theta'-\tilde{x}_2)^2+(1+\frac{r}{H}\cos\theta')^2\right]\tilde{T}\right) \ . \tag{4.24}$$

Next, we keep only terms such that the trace in (4.20) is of $\mathcal{O}\left(\frac{r}{H^2}\right)$. Considering Eqs. (4.23) and (4.24), one sees that $\Delta\mathcal{M}_{12}$ and $\mathcal{M}_{21}$ become independent of Ω and Ω' in this approximation, and therefore the two integrations over the solid angles just contribute a factor of $16\pi^2$.

Summing all these steps up, we can now write the trace formula of Eq. (4.20) in the desired fashion:

$$\mathsf{tr}\left(\Delta\mathcal{M}_{12}\mathcal{M}_{22}^{-1}\mathcal{M}_{21}\right) = T_E\frac{r}{H^2}2\int_{\tilde{\zeta}}\int_{\vec{\tilde{x}}_\parallel}\Delta\tilde{\mathcal{M}}_{12}(\tilde{\zeta},\vec{\tilde{x}}_\parallel)\tilde{\mathcal{M}}_{21}(\tilde{\zeta},\vec{\tilde{x}}_\parallel) + \mathcal{O}\left(\frac{r^2}{H^3}\right) . \tag{4.25}$$

The only dimensionful quantities in this equation are now T_E, r and H and the integral provides just the numerical value for the scaling. The propagators of the dimensionless tilded variables read in proper time representation

$$\begin{aligned}\Delta\tilde{\mathcal{M}}_{12}(\tilde{\zeta},\vec{\tilde{x}}_\parallel) &= \frac{1}{\pi^{\frac{3}{2}}}\int_0^\infty \mathrm{d}\tilde{S}\sqrt{\tilde{S}}\exp[-(1+\vec{\tilde{x}}_\parallel^2)\tilde{S}]\exp\left[-\frac{\tilde{\zeta}^2}{4\tilde{S}}\right]\\ \tilde{\mathcal{M}}_{21}(\tilde{\zeta},\vec{\tilde{x}}_\parallel) &= \frac{1}{2\sqrt{\pi}}\int_0^\infty \mathrm{d}\tilde{T}\frac{1}{\tilde{T}}\exp[-4\pi^2(1+\vec{\tilde{x}}_\parallel^2)\tilde{T}]\\ &\quad\times\exp\left[\frac{\tilde{\zeta}^2}{16\pi^2\tilde{T}}\right] .\end{aligned} \tag{4.26}$$

The twiddle sign over the matrix elements both indicates that they have become dimensionless through the rescaling with H as well as the fact that their trace in (4.25) only contributes the numerical constant to the order $\mathcal{O}\left(\frac{r}{H^2}\right)$ of the potential energy.

The remaining integrations in the trace expression can now be performed easily. The integral over $\tilde{\zeta}$ is purely Gaussian and the integral over $\vec{\tilde{x}}_\parallel$ is facilitated by the use of planar polar coordinates. At last, we perform the integration over the variables of the proper time representation $\tilde{T}$ and $\tilde{S}$.

The result is

$$\mathsf{tr}\left(\Delta\mathcal{M}_{12}\mathcal{M}_{22}^{-1}\mathcal{M}_{21}\right) = T_E\frac{1}{4\pi}\frac{r}{H^2} + \mathcal{O}\left(\frac{r^2}{H^3}\right) . \tag{4.27}$$

The energy of the configuration which is given by

$$E_{cas}(H) = -\frac{\hbar c}{T_E}\frac{1}{2}\mathsf{tr}\left(\Delta\mathcal{M}_{12}\mathcal{M}_{22}^{-1}\mathcal{M}_{21}\right), \tag{4.28}$$

consequently yields

$$E_{cas}(H) = -\frac{\hbar c}{8\pi}\frac{r}{H^2} + \mathcal{O}\left(\frac{r^2}{H^3}\right) . \tag{4.29}$$

The lowest order expansion coefficient agrees with recent results that were obtained by the use of different calculational techniques [24, 41].

Note that higher order terms could also be included in this formalism. To this end, higher order coefficients of the expansion of $\mathcal{M}_{22}^{-1}$ (cf. Eq.(4.15)) and higher order propagator traces have to be included.

Nevertheless we will restrict ourselves here to the lowest order term which is the only relevant term in the Casimir-Polder limit. Note that the Casimir-Polder limit of $\frac{r}{H} \ll 1$ is contrary to the limit accessible to the Proximity Force Approximation (PFA) [15, 16], since the PFA approximates the sphere by infinitesimally small flat segments and thus demands $\frac{r}{H} \gg 1$.

4.2.2 Arrangements for uniaxially corrugated surfaces

As we have shown, the spatial integrations over the surface of the sphere S_2 become trivial in the Casimir-Polder limit and thus contribute only a numerical factor. Due to this fact, the integrations over the remaining lateral coordinates $\vec{x}_\parallel$ on the plate (cf. Eq. (4.25)) could also be performed in momentum space since the plate itself is translationally invariant along these directions. However, in the next section we will extend our investigations to surfaces which are uniaxially structured along the direction x_1.

For this purpose it is feasible to rewrite Eqs.(4.25) and (4.26) with the 2-component p_2 in momentum space.

We get

$$\begin{aligned}\mathsf{tr}\left(\Delta\mathcal{M}_{12}\mathcal{M}_{22}^{-1}\mathcal{M}_{21}\right) &= \frac{T_E}{\pi}\frac{r}{H^2} \\ &\times \int_{\tilde{\zeta}}\int_{\tilde{p}_2}\int_{\tilde{x}_1} \Delta\tilde{\mathcal{M}}_{12}(\tilde{\zeta},\tilde{p}_2,\tilde{x}_1)\tilde{\mathcal{M}}_{21}(\tilde{\zeta},\tilde{p}_2,\tilde{x}_1) + \mathcal{O}\left(\frac{r^2}{H^3}\right) \ , \quad (4.30)\end{aligned}$$

with the associated propagators given in terms of modified Bessel functions of the second kind:

$$\begin{aligned}\Delta\tilde{\mathcal{M}}_{12}(\tilde{\zeta},\tilde{p}_2,\tilde{x}_1) &= \frac{1}{\pi}\frac{\sqrt{\tilde{p}_2^2+\tilde{\zeta}^2}}{\sqrt{1+\tilde{x}_1^2}} K_1\left(\sqrt{1+\tilde{x}_1^2}\sqrt{\tilde{p}_2^2+\tilde{\zeta}^2}\right) \\ \tilde{\mathcal{M}}_{21}(\tilde{\zeta},\tilde{p}_2,\tilde{x}_1) &= \frac{1}{2\pi} K_0\left(\sqrt{1+\tilde{x}_1^2}\sqrt{\tilde{p}_2^2+\tilde{\zeta}^2}\right) \ , \quad (4.31)\end{aligned}$$

after the execution of the integrals over $\tilde{S}$ and $\tilde{T}$.

Due to the simple structural dependency of the propagators on $\tilde{\zeta}$ and $\tilde{p}_2$, we can even further simplify the set of equations.

Defining $\tilde{q} = \sqrt{\tilde{p}_2^2 + \tilde{\zeta}^2}$, we get (4.30) as

$$\mathsf{tr}\left(\Delta\mathcal{M}_{12}\mathcal{M}_{22}^{-1}\mathcal{M}_{21}\right) = T_E\frac{2r}{H^2} \times \int_0^\infty \mathrm{d}\tilde{q}\int_{-\infty}^\infty \mathrm{d}\tilde{x}_1\,\tilde{q}\Delta\tilde{\mathcal{M}}_{12}(\tilde{\zeta},\tilde{p}_2,\tilde{x}_1)\tilde{\mathcal{M}}_{21}(\tilde{\zeta},\tilde{p}_2,\tilde{x}_1) + \mathcal{O}\left(\frac{r^2}{H^3}\right)\ , \quad (4.32)$$

where the propagators now read

$$\begin{aligned}\Delta\tilde{\mathcal{M}}_{12}(\tilde{q},\tilde{x}_1) &= \frac{1}{\pi}\frac{\tilde{q}}{\sqrt{1+\tilde{x}_1^2}}K_1\left(\tilde{q}\sqrt{1+\tilde{x}_1^2}\right)\\ \tilde{\mathcal{M}}_{21}(\tilde{q},\tilde{x}_1) &= \frac{1}{2\pi}K_0\left(\tilde{q}\sqrt{1+\tilde{x}_1^2}\right)\ .\end{aligned} \quad (4.33)$$

5 Scalar Casimir-Polder potential for corrugated surfaces

In the following section we will discuss how the Casimir energy can be obtained for a situation where the plate is not planar anymore but rather uniaxially structured along the direction x_1.

We choose the setup such that the structured surface still lies parallel to the $x_1 - x_2$ plane at $x_3 = 0$ (cf. Fig. 2).

Let $h(x_1)$ be a height function parametrising the structure such that a four-vector pointing onto the structured surface reads $x = (x_0, x_1, x_2, h(x_1))$. Again the plate should be considered as being infinitely extended along the directions x_1 and x_2.

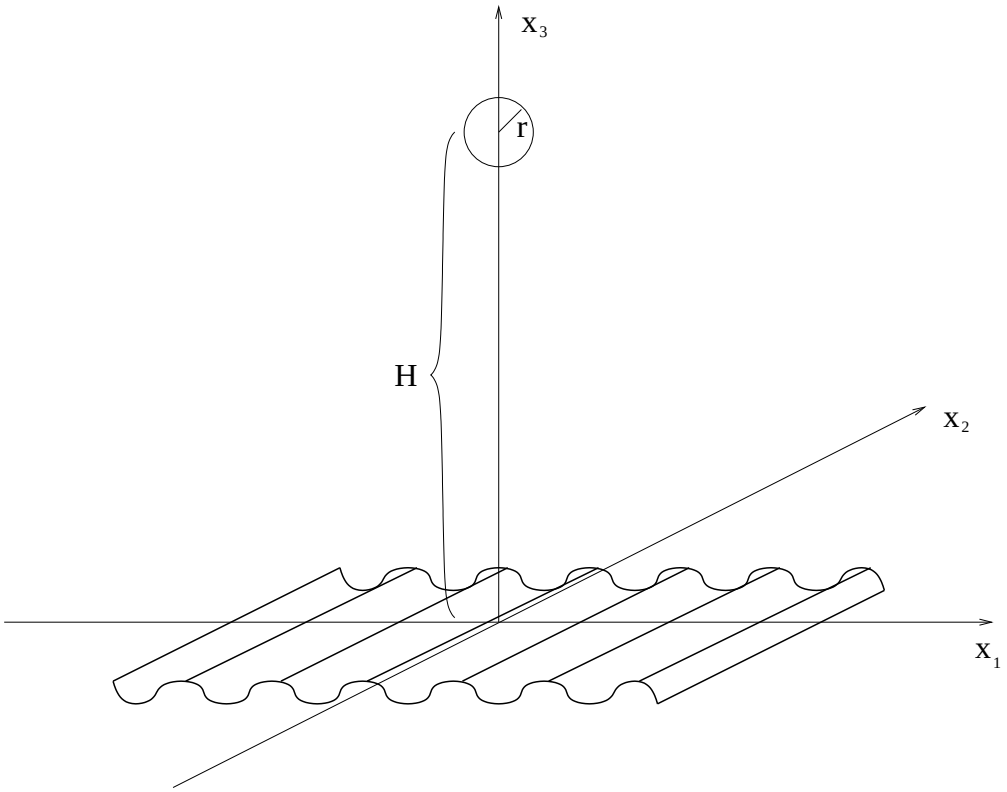

Figure 2: Sphere of radius r above a surface which is uniaxially structured along x_1. The mean distance between the centre of the sphere and the structure be H.

5.1 Setup

5.1.1 Inverse propagator on uniaxial structure

The main obstacle in the extension of the previous calculations to corrugated surfaces is the determination of the inverse propagator on the structured surface, $\mathcal{M}_{11}^{-1}$. The result for flat surfaces as given in Eq. (2.28) is easily obtained since $\mathcal{M}_{11}$ is translationally invariant along $\underline{x} = (x_0, x_1, x_2)$ and therefore diagonal in momentum space. $\mathcal{M}_{11}$ can thus be inverted in momentum space and transformed back to position space without major difficulties.

By contrast, a structured surface does not exhibit the translational invariance of the system in the direction of corrugation and the determination of the functional inverse of $\mathcal{M}_{11}$ becomes a difficult task even for the most simple case of scalar fields.

One could be lead to believe, though, that for periodically corrugated surfaces a similar recipe as for the evaluation of the inverse propagator on the surface of the sphere would apply. There, the expansion of the propagator in a complete set of functions together with the completeness relation for these functions allowed the evaluation of the expansion coefficients of the inverse propagator.

In a similar manner, one could think, it would hold that for a periodically corrugated surface an expansion of $\mathcal{M}_{11}$ as a Fourier sum and the usage of the completeness relation for the Fourier modes would provide us with coefficients of $\mathcal{M}_{11}^{-1}$. Unfortunately this is not the case.

Consider a surface structured along x_1, with a height function $h(x_1)$ parametrizing the structure. Then, taking into account only the relevant space dependencies, we have:

$$\mathcal{M}_{11} = \mathcal{M}_{11}\left(h(x_1) - h(x_1'), x_1 - x_1'\right) \ . \tag{5.1}$$

If we demand a periodic height function $h(x_1) = h(x_1 + \lambda)$ with a period λ and define new coordinates $\bar{x} = \frac{1}{2}(x_1 + x_1')$ and $\bar{z} = \frac{1}{2}(x_1 - x_1')$ then also the surface propagator is periodic in the new coordinate $\bar{x}$, i.e.

$$\mathcal{M}_{11}\left(\bar{x}, \bar{z}\right) = \mathcal{M}_{11}\left(\bar{x} + \lambda, \bar{z}\right) \ . \tag{5.2}$$

Thus the function can be expanded in Fourier modes with respect to the coordinate $\bar{x}$:

$$\mathcal{M}_{11}\left(\bar{x}, \bar{z}\right) = \sum_{k=-\infty}^{\infty} c_k(\bar{z}) \exp(\imath k\omega\bar{x}) \ , \tag{5.3}$$

with $\omega = \frac{2\pi}{\lambda}$ and $c_k(\bar{z}) = \frac{1}{\lambda}\int_0^\lambda \mathcal{M}_{11}\left(\bar{x}, \bar{z}\right) \exp(-\imath k\omega\bar{x})\mathrm{d}\bar{x}$.

Using a similar reasoning scheme as below Eq. (4.4) does, however, not apply since the expansion coefficients $c_k(\bar{z})$ are intrinsically dependent on the coordinates x_1 and x_1' and therefore the orthogonality relation for the exponential functions cannot be utilized.

For this reason, we choose a numerical approach in determining $\mathcal{M}_{11}^{-1}$ on the corrugated plate.

This is still highly nontrivial owing to the fact that $\mathcal{M}_{11}^{-1}$ is distribution-valued. For a stable numerical algorithm, the inversion strategy as well as the order of integrations have to be chosen with great care.

5.1.2 Potential for general uniaxial deformations

As argued in the previous section it is advisable not to determine $\mathcal{M}_{11}^{-1}$ directly for a structured plate, but rather calculate again the combined propagator $\Delta\mathcal{M}_{12}$.

To this end consider first the pendant of Eq. (4.4), which is the general equation determining $\mathcal{M}_{11}^{-1}$:

$$\int_{\vec{x}\in S_1} \mathcal{M}_{11}(\zeta,\vec{x}';\vec{x})\mathcal{M}_{11}^{-1}(\zeta,\vec{x};\vec{x}'') = \delta(\vec{x}'-\vec{x}'')\big|_{\vec{x}',\vec{x}''\in S_1} \ . \tag{5.4}$$

The integration over the surface in this case is defined as

$$\int_{\vec{x}\in S_1} = \int_{x_1}\int_{x_2} \sqrt{g(x_1)}\Big|_{x_3=h(x_1)} \ , \tag{5.5}$$

with the determinant of the induced metric $g(x_1) = 1 + (\partial_1 h(x_1))^2$.

Thus (5.4) explicitly reads

$$\int_{\vec{x}_\parallel} \sqrt{g(x_1)}\mathcal{M}_{11}(\zeta,\vec{x}_\parallel';\vec{x}_\parallel)\mathcal{M}_{11}^{-1}(\zeta,\vec{x}_\parallel;\vec{x}_\parallel'') = \frac{1}{\sqrt{g(x_1')}}\delta(\vec{x}_\parallel'-\vec{x}_\parallel'') \ . \tag{5.6}$$

We now multiply this equation from the left with a factor of

$$\sqrt{g(x_1'')}\mathcal{M}_{12}(\zeta,\vec{x}_\parallel'';\vec{x}_\parallel''',x_3''')$$

and integrate both sides of Eq. (5.6) over the lateral components $\vec{x}_\parallel''$. One finds that

$$\int_{\vec{x}_\parallel} \sqrt{g(x_1)}\mathcal{M}_{11}(\zeta,\vec{x}_\parallel';\vec{x}_\parallel)\Delta\mathcal{M}_{12}(\zeta,\vec{x}_\parallel;\vec{x}_\parallel''',x_3''') = \mathcal{M}_{12}(\zeta,\vec{x}_\parallel';\vec{x}_\parallel''',x_3''') \ , \tag{5.7}$$

where $\Delta\mathcal{M}_{12}$ explicitly includes the metric factor of the respective structure, i.e.

$$\Delta\mathcal{M}_{12}(\zeta,\vec{x}_\parallel;\vec{x}_\parallel'',x_3'') = \int_{\vec{x}_\parallel'} \sqrt{g(x_1')}\mathcal{M}_{11}^{-1}(\zeta,\vec{x}_\parallel;\vec{x}_\parallel')\mathcal{M}_{12}(\zeta,\vec{x}_\parallel';\vec{x}_\parallel'',x_3'') \ . \tag{5.8}$$

Since the matrix elements in the considered setup of uniaxial structures are still diagonal in p_2, we Fourier-transform Eq.(5.7) to position space in its 2-component. Dropping one $'$, Eq. (5.7) finally reads

$$\int_{x_1} \sqrt{g(x_1)}\mathcal{M}_{11}(\zeta, p_2, x_1'; x_1)\Delta\mathcal{M}_{12}(\zeta, p_2, x_1; x_1'', x_3'') = \mathcal{M}_{12}(\zeta, p_2, x_1'; x_1'', x_3'') \ . \quad (5.9)$$

As argued before, we cannot obtain the propagator $\Delta\mathcal{M}_{12}$ analytically. Yet we know $\mathcal{M}_{11}$ and $\mathcal{M}_{12}$, and thus Eq. (5.9) can be used in order to determine $\Delta\mathcal{M}_{12}$ for a structured surface numerically. Note, though, that the equation is still given in terms of dimensionful variables.

Following the same lines as in the previous section, we want to consider the dimensionless contribution of the propagator $\Delta\mathcal{M}_{12}$. Equation (5.9) is therefore rescaled and reads in terms of the dimensionless tilded variables[11]:

$$\int_{\tilde{x}_1} \sqrt{g(\tilde{x}_1)}\tilde{\mathcal{M}}_{11}(\tilde{q}, \tilde{x}_1'; \tilde{x}_1)\Delta\tilde{\mathcal{M}}_{12}(\tilde{q}, \tilde{x}_1) = \tilde{\mathcal{M}}_{12}(\tilde{q}, \tilde{x}_1') \ , \quad (5.10)$$

where now

$$\tilde{\mathcal{M}}_{11}(\tilde{\zeta}, \tilde{p}_2, \tilde{x}_1'; \tilde{x}_1) = \frac{1}{2\pi}K_0\left(\tilde{q}\sqrt{(\tilde{x}_1' - \tilde{x}_1)^2 + \left(\frac{h(\tilde{x}_1'H) - h(\tilde{x}_1H)}{H}\right)^2}\right) \ , \quad (5.11)$$

$$\tilde{\mathcal{M}}_{12}(\tilde{q}, \tilde{x}_1') = \frac{1}{2\pi}K_0\left(\tilde{q}\sqrt{(\tilde{x}_1')^2 + \left(\frac{h(\tilde{x}_1'H)}{H} - 1\right)^2}\right) \ , \quad (5.12)$$

and the metric factor

$$\sqrt{g(\tilde{x}_1)} = \sqrt{1 + (\partial_1 h(\tilde{x}_1 H))^2} \ . \quad (5.13)$$

Thus through rescaling, all distances are now given as multiples of H.

From our considerations of the plane-sphere scenario we know that the fluctuation-induced potential between the sphere and the corrugated surface

[11] Here we have included the factor of H appearing on the left hand side of Eq. (5.10) upon rescaling of the integration variable into the definition of the trace expression, see Eq. (5.14).

is obtained by evaluating[12]

$$\mathsf{tr}\left(\Delta\mathcal{M}_{12}\mathcal{M}_{22}^{-1}\mathcal{M}_{21}\right) = T_{\mathrm{E}}\frac{2r}{H^2}\int_0^\infty \mathrm{d}\tilde{q}\int_{-\infty}^\infty \mathrm{d}\tilde{x}_1\,\sqrt{g(\tilde{x}_1)}\tilde{q}\Delta\tilde{\mathcal{M}}_{12}(\tilde{q},\tilde{x}_1)\tilde{\mathcal{M}}_{21}(\tilde{q},\tilde{x}_1) + \mathcal{O}\left(\frac{r^2}{H^3}\right) . \quad (5.14)$$

The potential energy between the corrugated surface and the sphere will again be given by

$$E_{cas}(H) = -\frac{\hbar c}{T_E}\frac{1}{2}\mathsf{tr}\left(\Delta\mathcal{M}_{12}\mathcal{M}_{22}^{-1}\mathcal{M}_{21}\right) . \quad (5.15)$$

Equation (5.10) with its associated propagators (5.11) and (5.12) together with the trace expression (5.14) are now the starting point for our investigations of the two following section, where we will determine the induced potential in the cases of a sinusoidally shaped surface numerically.

We use Eq.(5.10) to extract the unknown propagator $\Delta\tilde{\mathcal{M}}_{12}$ and apply our result in Eq.(5.14) in order to determine the trace over all propagators and thereby the energy of the configuration.

Let us stress that though the method applied here is valid only for $\frac{r}{H} \ll 1$, it is non-perturbative. Thus there is no need to assume that the amplitude of the corrugation is small compared to the distance between sphere and plate as required in other approaches (e.g. [30]).

Also we stress again that the method probes parameter ranges inaccessible to the Proximity Force Approximation (PFA) [15, 16] since the latter is only reliable in the limit of $\frac{r}{H} \gg 1$.

5.2 Sinusoidally structured surfaces

5.2.1 Prerequisites

As an exemplary application of our method we want to consider the fluctuation-induced potential between a sphere and a sinusoidally corrugated surface.

We parametrize the structure by the one-dimensional height function

$$h(x_1) = A\sin(\omega(x_1+\phi)) , \quad (5.16)$$

and thus have the means of varying the structure amplitude A as well as its frequency ω. Since in our formulation the location of the centre of the sphere with respect to the direction of corrugation is fixed, a phase ϕ is introduced

[12] Again, due to the symmetry of the problem we have $\tilde{\mathcal{M}}_{21} = \tilde{\mathcal{M}}_{12}$ and therefore the structure of $\tilde{\mathcal{M}}_{21}$ can be read off Eq. (5.12) .

to *simulate* the movement of the sphere through a continuous displacement of the structure itself.

With the height function $h(x_1)$ of the corrugation we can now give explicit representations of the propagators and the metric factor of Eqs. (5.11-5.13).

In terms of the rescaled variables we have the propagators

$$\tilde{\mathcal{M}}_{11}(\tilde{q},\tilde{x}_1';\tilde{x}_1) = \frac{1}{2\pi}K_0\left(\tilde{q}\sqrt{(\tilde{x}_1'-\tilde{x}_1)^2+\left(\frac{\tilde{A}\sin(\tilde{\omega}(\tilde{x}_1'+\phi))-\tilde{A}\sin(\tilde{\omega}(\tilde{x}_1+\phi))}{H}\right)^2}\right) \tag{5.17}$$

and

$$\tilde{\mathcal{M}}_{12}(\tilde{q},\tilde{x}_1') = \frac{1}{2\pi}K_0\left(\tilde{q}\sqrt{(\tilde{x}_1')^2+\left(\frac{\tilde{A}\sin(\tilde{\omega}(\tilde{x}_1'+\phi))}{H}-1\right)^2}\right) . \tag{5.18}$$

The metric factor of the surface integration reads

$$\sqrt{g(\tilde{x}_1)} = \sqrt{1+[\tilde{A}\tilde{\omega}\cos(\tilde{\omega}(\tilde{x}_1+\phi))]^2} . \tag{5.19}$$

Note that all tilded variables again indicate that they are given in units of the mean distance H.

In the following we will discuss a possible discretization of these functions in order to obtain the Casimir energy of the setup numerically.

5.2.2 Numerical implementation

In this section, we drop the "$\sim$" marking the dimensionless quantities in order not to clutter up the notation. Since the space between surface and sphere along the direction x_3 is denoted by the mean distance H in the formulation, we can also drop the index of x_1 without danger of confusion and thus set $x_1 \equiv x$ from now on.

For the numerical evaluation of the unknown propagator $\Delta\mathcal{M}_{12}$, first of all Eq.(5.10) is discretized in its spatial arguments x' and x. To this end we approximate the integral over the spatial variable through a left Riemann

sum which is defined as[13]:

$$\int_{-\infty}^{\infty} \mathrm{d}x f(x) \approx \sum_{i=0}^{N-1} \Delta x f(x_i) \ ,$$

where N_x is the number of nodes and $\Delta x = x_{i+1} - x_i$ the step size of the discretization, respectively.

Naturally the integration over x originally running from $-\infty$ to $+\infty$ must be cut off at some finite value. Since the sphere is located at the position $x = 0$ above the surface, we choose a symmetric cutoff at the positive variable L_x. With $x_i = -L_x + i\Delta x$, we have for the left and the right interval limits $x_0 = -L_x$ and $x_{N-1} = L_x - \Delta x$ and thus for the step size $\Delta x = \frac{2L_x}{N_x}$.

Note that since in experiments the plate extension of course is not infinite, the parameter L_x can even be associated with a physical quantity.

We thus write Eq.(5.10) as

$$\sum_{i=0}^{N_x-1} \Delta x \sqrt{g_i} \mathcal{M}_{11,ji}(q) \Delta \mathcal{M}_{12,i}(q) = \mathcal{M}_{12,j}(q) \ , \tag{5.20}$$

where the variables x and x' have been replaced by the subscript indices i and j, respectively, whereas the momentum variable q remains continuous for the time being. The subscript indices have been introduced for easier readability and should be understood as $\mathcal{M}_{\alpha\beta,ji} = \mathcal{M}_{\alpha\beta}(x_i, x_j)$, $\mathcal{M}_{\alpha\beta,i} = \mathcal{M}_{\alpha\beta}(x_i)$ and $\sqrt{g_i} = \sqrt{g(x_i)}$, with the definition of x_i as given above.

Thus, through the process of discretization, $\mathcal{M}_{11}$ now acquires a matrix structure containing the respective nodes along x' and x in its row and column entries, whilst $\mathcal{M}_{12}$ and $\sqrt{g}$ assume the form of a vector.

Yet, one has to be careful with the choice of discretization points in x and x' due to the fact that the zeroth Bessel function appearing in the definition of $\mathcal{M}_{11}$ diverges at the origin (cf. Eq. (5.17)). Therefore we choose the nodes in x' and x such that they are separated by an offset Δs. This offset should then of course not be a multiple of the chosen discretization step size in order not to hit the pole.

Also, in order to avoid a bias towards too high or too low numerical values of $\mathcal{M}_{11}$ due to the offset, the complete evaluation of $\Delta\mathcal{M}_{12}$ is done once with a positive and once with a negative offset Δs. Finally we work with the mean value of both results.

[13]Replacing the integration over x through a left Riemann sum is admittedly a fairly crude approximation to the integral and there exists of course an abundance of more sophisticated methods. Nevertheless already a simple Riemann sum yields rather accurate results as we will see shortly. Therefore this approximation shall suffice for our first numerical studies.

Now, in order to obtain $\Delta\mathcal{M}_{12,i}$, the discretized propagator $\mathcal{M}_{11,ji}$ together with the metric factor $\sqrt{g_i}$ is inverted numerically and multiplied by the vectorial term $\mathcal{M}_{12,j}$ on the right hand side of Eq. (5.20). This quantity needs to be computed for all possible positive values of the momentum q. Thus, the propagator $\Delta\mathcal{M}_{12}$ itself assumes a matrix form upon discretization of the continuous momentum variable.

With $\Delta\mathcal{M}_{12}$ given, now the potential energy of the configuration is computed.

The discretized version of Eq. (5.14) reads

$$\mathsf{tr}\left(\Delta\mathcal{M}_{12}\mathcal{M}_{22}^{-1}\mathcal{M}_{21}\right) = T_{\mathrm{E}}\frac{2r}{H^2}\sum_{k=0}^{N_k-1} q_k\,\Delta q\sum_{i=0}^{N_x-1}\Delta x\sqrt{g_i}\,\Delta\mathcal{M}_{12,ik}\,\mathcal{M}_{21,ik}\ . \quad (5.21)$$

The approximation of the momentum integration is carried out analogously to the spatial case (i.e. we use a left Riemann sum) except for the fact that the momentum integration only runs over positive values. We label the lower cutoff of the momentum integration as L_q and the upper cutoff as R_q. The step size Δq is consequently given as $\Delta q = \frac{L_q+R_q}{N_q}$, where N_q is the number of nodes along q.

Yet, again owing to the fact that the Bessel function K_0 diverges at the origin, we cannot choose the value 0 itself as the smallest node L_q in the discretization of the momentum integration.

Finally, using Eq.(5.15), we see that the Casimir energy of the configuration is given by

$$E_{cas}(H) = -\hbar\,c\,r\frac{1}{H^2}\sum_{k=0}^{N_k-1} q_k\,\Delta q\sum_{i=0}^{N_x-1}\Delta x\sqrt{g_i}\,\Delta\mathcal{M}_{12,ik}\,\mathcal{M}_{21,ik}\ . \quad (5.22)$$

Note that this formula holds for general uniaxial deformations.

5.2.3 Parameter choice and validity limits

As a check on the validity and precision of the numerical implementation we have the limiting case of a flat surface as presented in section 4, since this limit is known analytically. We thus use the comparison to the planar case in order to tune our parameters of the discretization and test their range of validity.

Equations (5.20) and (5.22) for a flat surface S_1 read

$$\sum_{i=0}^{N_x-1}\Delta x\,\mathcal{M}_{11,ji}(q)\,\Delta\mathcal{M}_{12,i}(q) = \mathcal{M}_{12,j}(q) \quad (5.23)$$

and

$$E_{cas}(H) = -\hbar\, c\, r \frac{1}{H^2} \sum_{k=0}^{N_q-1} q_k\, \Delta q \sum_{i=0}^{N_x-1} \Delta x\, \Delta \mathcal{M}_{12,ik}\, \mathcal{M}_{21,ik}\ . \tag{5.24}$$

As outlined before, an offset $\pm\Delta s$ between the nodes x and x' is introduced to circumvent divergencies, thus first of all the effect of this offset is studied.

One should not forget, though, that the most adequate choice of Δs is not unique but rather depends on the used step size Δx. Choosing Δs too small with respect to the step size Δx amounts to high values along the diagonal of $\mathcal{M}_{11,ji}$ and thus to small values for $\Delta\mathcal{M}_{12,i}$ since $\Delta\mathcal{M}_{12,i}$ is proportional to the inverse of $\mathcal{M}_{11,ji}$ (cf. Eq. (5.23)).

On the other hand, choosing Δs too big with respect to Δx consequently yields too high values for $\Delta\mathcal{M}_{12,i}$. As it turns out, the most suited[14] choice for Δs is about $\frac{1}{2}$ of the used step size Δx , since it yields the best agreement with the analytical values of $\Delta\mathcal{M}_{12}$.

Among all parameters of the discretization, the choice of L_x and Δx depends for the most part on the available computing power. This is due to the fact that the values for L_x and Δx determine the size of the matrix $\mathcal{M}_{11,ji}$ which needs to be inverted for the computation of the potential. For our studies using MATHEMATICA 6.0, we restrict ourselves to a maximum precision involving at most a 126×126 matrix in $\mathcal{M}_{11,ji}$.

As already mentioned earlier, the introduction of a seemingly unwanted cutoff L_x is not inconvenient. In fact one can associate the parameter L_x with the finite extension of the plate and tune it in order to study boundary effects. At first, however, we aim at minimizing the influence of the boundaries.

For fixed values of H and Δx it turns out to be a good compromise to choose the upper and lower bounds of the spatial integration $\pm L_x$ around the value of the maximal separation between surface and sphere. This assures that the sphere is always closer to the centre of the structure than to its edges. With the selected maximal dimension of the matrix $\mathcal{M}_{11,ji}$, this immediately fixes the step size Δx as well.

At last, in order to find a reasonable choice for the step size of the q-integration as well as its upper and lower cutoffs, it is suitable to consider

[14] As a side remark we note that very small step sizes Δx result in too high values for the potential E_{cas}. In a way this countervails the effect of small offsets Δs. This is an unwanted effect since it makes it impossible to check if the chosen combination of Δs and Δx indeed is the one yielding the best numerical results. It is therefore desirable to circumvent the introduction of Δs in the first place by an appropriate regularization of the Bessel function appearing in $\mathcal{M}_{11}$ itself. This option will be further discussed in section 5.3.1.

the potential of Eq. (5.24) without performing the momentum integration. Defining the expression

$$f(q) = q \sum_{i=0}^{N_x} \Delta x \sqrt{g_i} \Delta \mathcal{M}_{12,i}(q) \mathcal{M}_{21,i}(q) \ , \tag{5.25}$$

we study the behaviour of $f(q)$ to find appropriate lower and upper cutoffs L_q and R_q. For given parameters of the spatial discretization, $f(q)$ is peaked around some momentum q and thus values for L_q, R_q as well as the step size of the momentum integration Δq can be picked depending on the desired degree of precision[15]. In the following, we always choose as dimensionless parameters for the momentum integration $L_q = 0.01$, $R_q = 4$ and $\Delta q = 0.04$. The parameters corresponding to the spatial discretization are adjusted according to the investigated setup.

Now, with reasonable values for the discretization parameters at hand, we check on the agreement of our numerics with the analytical result for the energy in the limit of a flat surface. For a vanishing structure amplitude A, the numerical results should reproduce the value of the potential for the sphere (S) - plane (P) configuration as given in Eq.(4.29):

$$E_{\mathrm{SP}}(H) = -\frac{1}{8\pi} \frac{\hbar c r}{H^2} \approx -0.03979 \frac{\hbar c r}{H^2} \ . \tag{5.26}$$

It is reasonable to assume that the degree of agreement achieved in the planar case approximately transfers to the case of non-planar surfaces, since no further discretization parameters come into play. The degree of congruence achieved by the parameters as used in the following section is discussed in Appendix C.2.

At last we would like to note that a further test on the implementation results from the fact that for a diverging structure frequency ω the sphere does not "see" the slots of the structure. Thus for separations $H \sim A$ the structured surface must behave like a planar surface at reduced mean height $H' = H - A$ in the limit of $\omega \to \infty$.

5.2.4 Results

As argued in section 5.2.1, we introduce a phase ϕ in the definition of the height function in order to extract the value of the potential for each point above the structure. For a sinusoidally shaped surface, it makes sense to consider the parameter range $\phi \in (-\pi, \pi]$.

[15] An exemplary graph showing the qualitative behaviour of $f(q)$ is given in Appendix C.1

Note that through the variation in ϕ, the actual shape of the structure is continuously modulated while the sphere itself stays fixed at the position $x = 0$. Therefore the boundary effects resulting from the finite plate size contribute by the same amount for every value of ϕ. Thus, for the case of vanishing boundary effects, the variation of ϕ can be associated with the movement of the sphere above an infinitely extended structure along the direction x.

In the following we want to study the shape of the potential along the direction of corrugation as well as the behaviour of the potential for varying separation between the surface and the sphere. Modulated frequencies of the structure function will also be accounted for.

Note, however, that to the end of studying the behaviour of the potential for varying mean separation it is no longer favourable to choose the mean distance H as a scale since we want the structure amplitude as well as the frequency to be fixed for decreasing H. Instead, the structure amplitude A is the relevant scale for the frequency ω, whilst the edges of the plate L_x and the step size Δx scale with[16] $H - A\sin(\omega\phi)$. This assures that the steps along x are adjusted reasonably: for small separations between sphere and plate the nodes along x lie close, whereas for bigger distances the discretization points are spread more coarsely. The edges of the corrugated plane converge as $H \to 0$, assuring that the sphere always "sees" the same number of nodes N_x.

In order to present our numerical results clearly, we write Eq. (5.22) as

$$\begin{aligned} E_{cas}(H) &= -\hbar c r \frac{1}{H^2} \sum_{k=0}^{N_q-1} q_k \Delta q \sum_{i=0}^{N_x-1} \Delta x \sqrt{g_i}\, \Delta\mathcal{M}_{12,ik}\, \mathcal{M}_{21,ik} \\ &\equiv \hbar c r \alpha \,, \end{aligned} \tag{5.27}$$

where we have introduced a parameter α characterizing the potential strength[17].

[16] When scaling L_x and Δx with the distance between surface and sphere, also the scaling of the parameters of the momentum integration L_q, R_q and Δq has to be adapted.

[17] Note, that the definition of α explicitly includes the minus sign appearing in E_{cas}. This makes it easier to combine the height function and α in one plot.

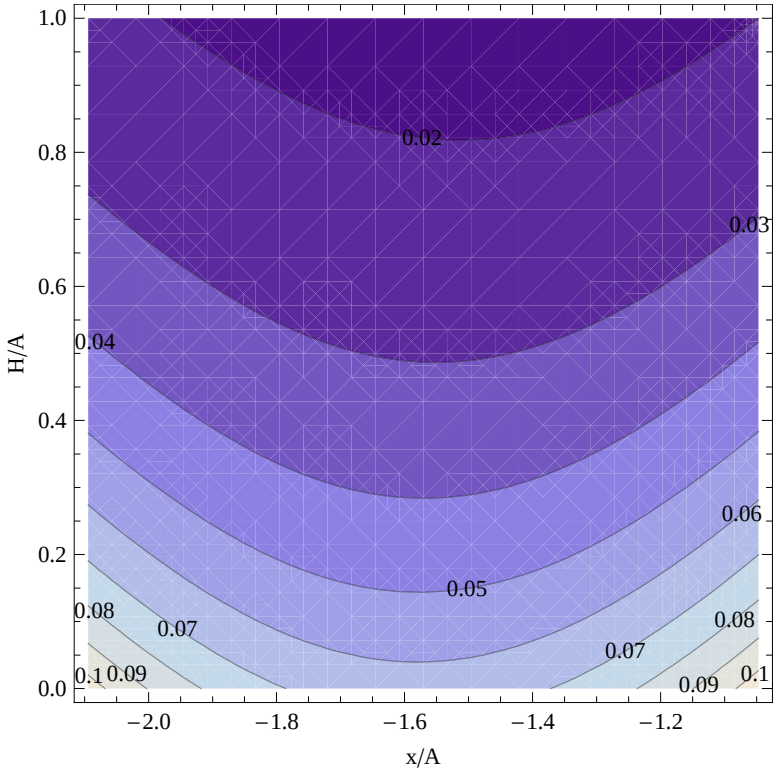

Figure 3: Lines of equal potential α inside a minimum of the sinusoidal structure, i.e. around $x = -\frac{\pi}{2}$ are shown as a function of the mean distance H scaled with the amplitude A of the corrugation. The value of the potential strength parameter α as defined in Eq. (5.27) is given at the respective contours and is graded graphically in between from lighter colours (high α) to darker colours (low α). The step size in spatial direction Δx is 0.5 in units of A, while the total size of the surface is $2L_x = 2\pi$ in multiples of A. The values along the direction of corrugation lie between $-\frac{2\pi}{3} \leq x/A \leq -\frac{\pi}{3}$. The frequency of the considered sinusoidal corrugation is chosen as $\omega/A = 1$. One can see that the equipotential lines resemble the shape of the structure trough itself and that the gaps between the contours widen for increasing ratios of H/A, highlighting the strong distance dependency of the Casimir force. However, in the contour plot only a very small number of nodes $N_x = 12$ can be used within a reasonable frame of computing time. The small number of discretisation nodes also causes the slight asymmetry of the equipotential lines. Thus the graph shows only the qualitative behaviour of α and for quantitative studies the lines have to be investigated separately (cf. Figs. 4 and 5).

In Figure 3, equipotential lines for several ratios of mean distance to amplitude inside a structure trough are shown along the direction of corrugation x. It can be seen that the potential varies only moderately for greater ratios H/A and diversifies stronger when H becomes very small with respect to the corrugation amplitude. For $H/A > 1$ the gaps between the equipotential lines become continuously wider and are thus not shown in the graph for the sake of lucidity. Around $H/A = 0.28$ above the absolute minimum at $x = -\frac{\pi}{2}$, the value of $\alpha \approx 0.04$ is assumed which corresponds to the value of α for a planar surface (cf. Eq. (5.26)). The slight asymmetry in the uppermost equipotential lines in the graph is ascribed to the use of a left Riemann sum within the discretization (cf. section 5.2.2).

Since the calculation of the lines of equal potential as presented in Fig. 3 is very time-consuming with MATHEMATICA, it can only be done for a rather low number of discretization nodes N_x and therefore yields only qualitative results.

In Figs. 4 and 5 we thus give the value of α along the x-direction for two selected ratios of A/H with a relatively high number of nodes $N_x = 80$. For easier readability, the shape of the structure function itself is included in the plot.

In Fig. 4, the mean distance H between the centre of the sphere and the structure is chosen to be twice as large as the structure amplitude A. One sees that the shape of the potential in this case resembles the shape of the structure function. However, it is already well recognizable that the energy between structure and sphere grows rapidly for shorter separations. This becomes even more obvious in Fig. 5, where the maximal amplitude A becomes 0.9 in units of H.

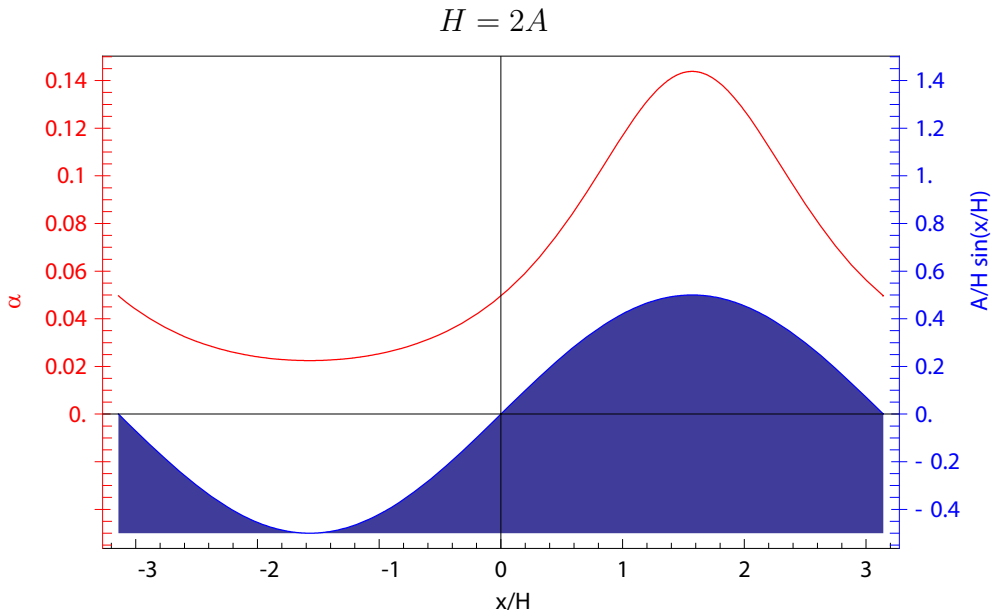

Figure 4: The potential strength parameter α as defined in Eq.(5.27) is given for every point above a sinusoidal structure with $x/H \in [-\pi, \pi]$ and $\omega/H = 1$ (upper line in red, scale on the left hand side), where H denotes the mean distance between surface and sphere. Since α cannot become smaller than 0, the scale on the right hand side does not show negative values. The course of the structure itself is depicted by the blue shaded area at the bottom. The corresponding height of the structure in units of H can be read off the blue scale on the right hand side. In this figure, the ratio of structure amplitude and mean distance is chosen as $A/H = 0.5$. The parameters of the spatial integration amount to $L_x = 2$ and $\Delta x = 0.05$ in units of H, respectively. The curve depicting the values of α resembles a slightly deformed sinusoidally shape, indicating that the sphere locally sees an almost flat plate.

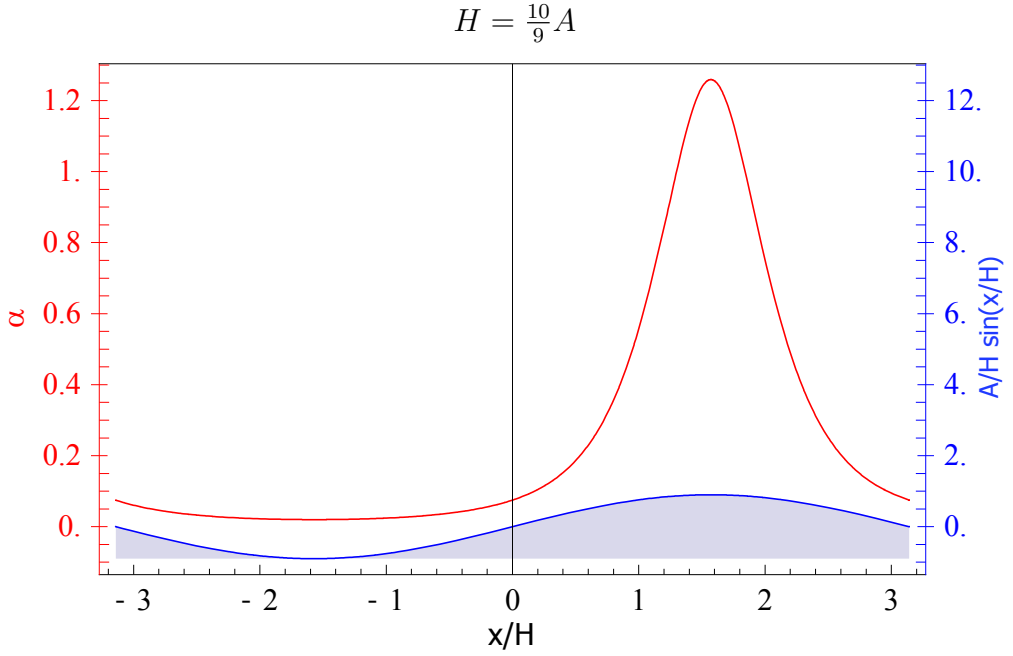

Figure 5: The potential strength parameter α as defined in Eq.(5.27) is given for every point above a sinusoidal structure with $x/H \in [-\pi, \pi]$ and $\omega/H = 1$ (upper line in red, scale on the left hand side) with H denoting the mean distance between surface and sphere. The course of the structure itself is depicted by the blue shaded area at the bottom. The corresponding height of the structure in units of H can be read off the blue scale on the right hand side. The ratio between amplitude and mean separation in this figure is $A/H = 0.9$. The parameters of the spatial integration amount to $L_x = 2$ and $\Delta x = 0.05$ in units of H. The curve depicting the course of α deviates drastically from a sinusoidal shape, accentuating the strong distance dependency of the Casimir force. Note the scale for the parameter α in this graph differs by a factor of 10 with respect to the scale as used in Fig. 4.

Next, we study the behaviour of the Casimir potential for varying mean separation between structure and sphere and compare it to the analytically known value for a sphere and a planar surface (cf. section 4). In particular we consider the potential values above a structure trough and an inflexion point of the structure along vertical lines with respect to the structure.

Above the structure trough, we expect the potential to approach the value of the corresponding planar case in the limits $H \ll A$ and $H \gg A$. In the first case, the alteration of the structure function becomes arbitrarily small and thus the sphere sees an almost flat plate. In the second case, the influence of the corrugation diminishes due to the strong decline of the Casimir force with the distance. For the same reason the normalized potential parameter should become 1 for $H \gg A$ above the point of inflexion.

Figure 6 depicts the deviation of the potential strength parameter α above an inflexion point of the structure with respect to the potential parameter α_P for a planar surface laid through the point of inflexion. The ratio α/α_P is given for three different values with respect to the frequency of the structure function. The setup is chosen such that at the upper limit of the curve corresponding to $H/A = 3$, the half length of the plate $L_x = \pi$ in units of A, assuring that the mean separation between surface and sphere is smaller than the distance between the sphere and the edges of the plate. This secures that edge effects are small. One can see that the potential induced by the structure begins to deviate considerably from the planar case as $H/A \to 0$. Also one finds that the degree of discrepancy increases drastically for greater ω since the gradient of the structure function increases with ω and thus the structure comes closer to the sphere. Since in the limit $H/A \to 0$ the space between the corrugated surface and the sphere at the inflexion point is always smaller than the distance between the sphere and a planar surface through the point of inflexion, the normalized potential parameter actually becomes considerably larger than $\alpha/\alpha_p = 1$.

Figure 7 shows the potential strength parameter α normalized to its value for a flat plate located at the minimum of the structure. Again, the ratio is given with respect to three different frequencies of the height function. All in all this can be looked upon as the sphere approaching the surface from a vertical direction and moving into a structure minimum. One sees that the maximum of the deviation is reached for $H \sim A$ and further that the deviation advances rapidly for higher modulation frequencies. This is ascribed to the fact that the vertical components of the forces induced in the setup increase for higher ω. Note that the variation in ω also shifts the position of the maximum of α/α_P to lower values of H/A. This is due to the fact that the sphere "sees" the limit of a planar surface later for higher values of ω.

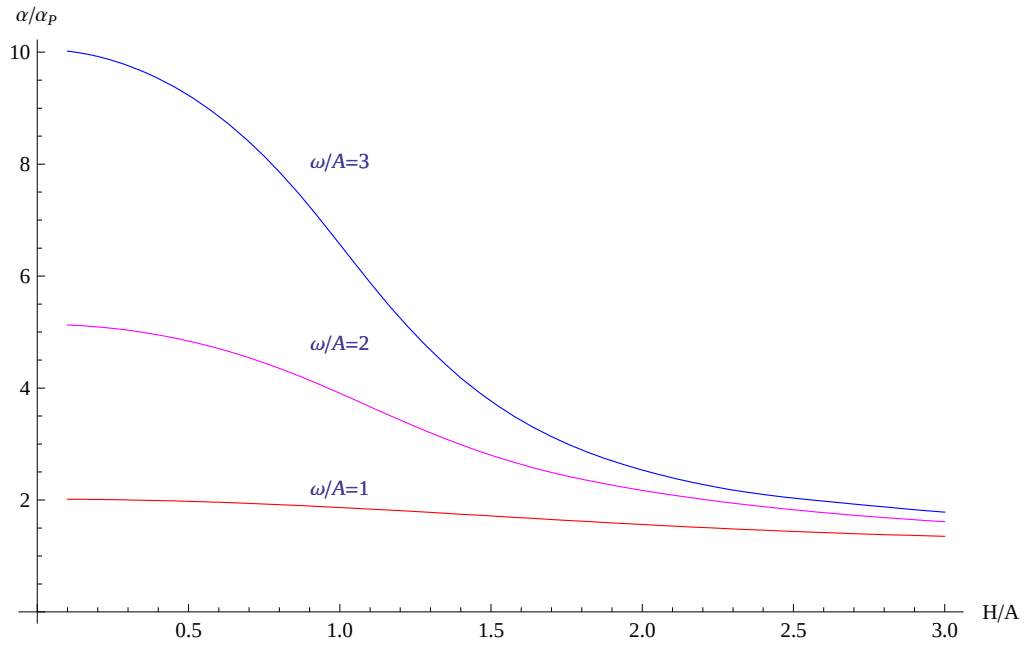

Figure 6: This graph shows the Casimir-Polder energy for a sinusoidally structured surface relative to the planar case above an inflexion point (i.e. $\phi = 0$) of the structure with amplitude A within the range of a dimensionless mean separation $3 \geq H/A \geq 0.1$. The potential strength parameter α is normalized to the value of the parameter for a planar surface located at mean distance $H = 0$, called α_P. The red (bottom), magenta (middle) and blue (top) curves show α/α_P as a function of the fraction H/A for $\omega/A = 1, 2, 3$, respectively. The step size Δx along the spatial direction and the spatial cutoff L_x are 0.1 and π in units of H, respectively. Thus the edges of the surface as well as the discretization nodes converge with decreasing separation between surface and sphere. In the graph one sees that the value of α/α_P increases articulately for higher values of ω. As $H/A \to 0$, the normalized potential strength parameter assumes values that are considerably larger than 1 since the gap between corrugated surface and sphere is smaller than the distance between the sphere and a planar surface through the inflexion point.

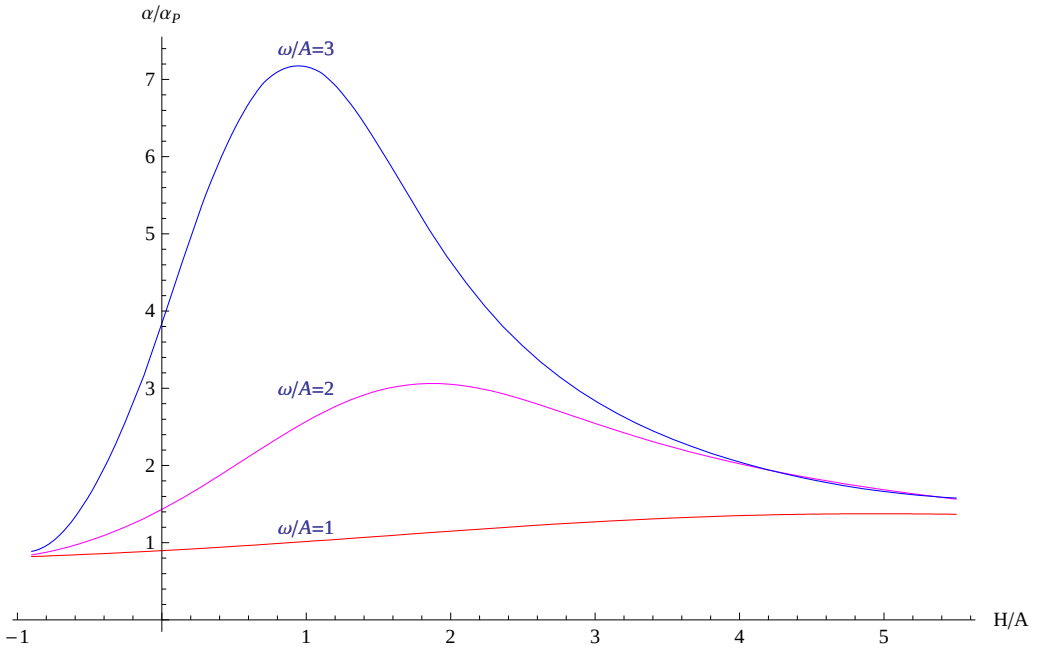

Figure 7: This graph shows the deviation of the Casimir-Polder energy for a sinusoidally shaped surface from the planar case above a structure trough for dimensionless mean separations $5.5 \geq H/A \geq -0.9$, where A is the amplitude of the structure. The potential strength parameter α is normalized to the value of the parameter for a planar surface α_P located at $H = -A$. The red (bottom), magenta (middle) and blue (top) curves refer to $\omega/A = 1, 2, 3$, respectively. The step size Δx along the spatial direction is 0.5 and the spatial cutoff $L_x = 2\pi$ in units of $H+A$, respectively. Thus the edges of the surface as well as the discretization nodes converge with decreasing separation between surface and sphere. The maximal deviation with respect to the planar case is met when H and A become of the same order of magnitude. For greater frequencies ω, the trough becomes narrower and thus the potential deviates from the planar case more drastically. Also the point of maximal deviation is shifted towards smaller H/A as ω/A increases, since the sphere perceives the limit of the flat plane at a later point. For $H/A \to -1$, the alteration of the structure function becomes arbitrarily small and thus $\alpha/\alpha_P \to 1$.

5.3 Improvements and extensions in the scalar and gauge field context

5.3.1 Alternative discretization

As mentioned in footnote 14 on page 43, the introduction of the shift Δs between the discretization nodes along the spatial direction is not favourable. There we argued, that Δs can not be chosen arbitrarily with respect to the step size Δx. However, within the discretization using Δs, the analytic value for the Casimir-Polder potential is expected to be obtained in the limit of an infinite number of discretization nodes $N_x \to \infty$, whilst $\Delta s \to 0$. In practice this amounts to the necessity of choosing some factor $c = N_x \, \Delta s$ as a working basis for the calculations of the potential. But though c can be tuned such that the analytically known value for the planar case is reproduced to an arbitrarily high degree of precision, it remains always unclear if the chosen combination of N_x and Δs is ideal or if an even better one can be found.

Thus we want to present an alternative discretization that circumvents this flaw. Instead of shifting the nodes of x and x' relative to each other in order to assure a non-vanishing argument of the Bessel function in $\mathcal{M}_{11}$, one can instead regularize the Bessel function itself.

In the limit of small arguments z, it holds for the modified Bessel function K_0 that $K_0(z) \sim -\ln(z)$ [42]. Therefore it seems to be an apt regularization to set

$$\mathcal{M}_{11}(z) = \begin{cases} \frac{1}{2\pi} K_0(z) & , z > \epsilon \\ -\frac{1}{2\pi} \ln(z + \epsilon) & , z \leq \epsilon \end{cases} , \tag{5.28}$$

where z now refers to the whole argument of the propagator as given in Eq. (5.11). By this, the nodes in x and x' can be chosen on top of each other and the new parameter $\epsilon > 0$ takes the role of the offset Δs.

With (5.28), now the analytical value of the discretized propagator $\mathcal{M}_{11}$ and the Casimir-Polder potential is again obtained in the limits $N_x \to \infty$ and $\epsilon \to 0$. However, in contrast to the discretization using the offset Δs, the behaviour of $\mathcal{M}_{11}$ can be studied for arbitrary fixed values of ϵ in the limit $N_x \to \infty$. The optimal value of ϵ with respect to the choice of a finite N_x can then be extrapolated from these studies.

5.3.2 Arbitrarily corrugated surfaces and modified boundary conditions

The evaluation scheme of section 5.2 is now in principle valid for any periodic uniaxial deformation. Arbitrary periodic structure functions can be decomposed into their Fourier modes and thereby the problem is reduced again to

the setup of sinusoidal shapes as already considered in section 5.2.

However, for non-smooth structure functions such as sawtooth or step functions the available numerical precision becomes crucial. There, an adequately small step size for the spatial discretization has to be chosen to avoid the occurrence of discretization artifacts at the points of large gradients. Within the frame of an implementation in MATHEMATICA, investigations of this kind therefore yield only qualitative results.

As a side remark we want to mention that our method can also be generalized to the case of biaxially corrugated surfaces. Two-dimensional deformations, however, demand considerably more numerical effort since the matrix inversion needed for the computation of $\Delta\mathcal{M}_{12}$ has to be performed with respect to two spatial variables. Furthermore, 2D corrugations imply a further integration over the second lateral coordinate in the trace expression (cf. Eq. (4.25)). But besides the increased numerical effort no principle obstruction is met.

Also an extension of this method to pure Neumann boundary conditions as well as interpolations[18] between Dirichlet and Neumann or even unlike[19] boundary conditions is possible. With the Green's function for the Neumann problem (cf. Eq. (2.18)), the inverse of the propagators on the surfaces and the respective propagators between the surfaces can be evaluated along the lines of this section and the potential energies can consequently be evaluated.

5.3.3 Full gauge field

In this chapter we have presented a simple and efficient way of how to calculate fluctuation-induced forces for a Dirichlet scalar field between a sphere and a uniaxially corrugated surface with a general periodic structure function.

However, in order to obtain classical Casimir-Polder potentials in the sense of fluctuation-induced potentials between actual atoms and a surface, a calculation for fluctuating scalar fields does not suffice. As argued in the beginning of section (2.2.2), a calculation in terms of one Dirichlet and one Neumann scalar field delivers the potential for the full electromagnetic field if and only if the setup is translationally invariant in at least one spatial direction. Since the choice of a sphere as one of the surfaces in the setup breaks the invariance in *all* spatial directions, scalar fields cannot account

[18] Interpolations between Dirichlet and Neumann boundary conditions are also referred to as Robin boundary conditions.

[19] By unlike boundary conditions we refer to the cases where Dirichlet boundary conditions are implemented on the sphere while Neumann boundary conditions are used on the surface and vice versa.

anymore for the behaviour of the full gauge field.

Moreover, studying the characteristics of an actual atom in front of a structured surface and thereby the explicit comparison with the experimental results [28] as described in the introduction of this thesis demands the use of proper boundary conditions of the electromagnetic fields on the atom.

It is thus desirable to use the techniques of this section in a formulation for fluctuating electromagnetic fields with general dielectric surfaces similar to the one reviewed in Appendix B. However the expressions for the propagators derived within this formulation are not applicable for our formulation since they only apply to surfaces whose corrugation can be parametrized by a height function of the lateral coordinates. A sphere unfortunately does not match this classification.

6 Résumé and outlook

In this analysis we aimed at the development of a simple, non-perturbative calculational scheme for Casimir-Polder potentials in the case of arbitrarily structured surfaces.

To this end we first reviewed the Quantum Field Theoretical treatment of fluctuating scalar fields with boundaries. Essentially, the fluctuation constraints are inserted via a δ functional into the generating functional $\mathcal{Z}$ of the theory. Through the Fourier transformation of the δ functional constraint, a set of auxiliary fields is introduced which is only defined on the surfaces themselves. Evaluating the Gaussian integrations over the physical and the auxiliary fields then yields a trace log formula for the Casimir energy and force of the system. The determination of the fluctuation-induced energy is therefore reduced to the evaluation of the propagators of the respective theory on and in between the surfaces. Thus, the Casimir energy itself is essentially given by the sum of every possible propagation cycle. As a first application of this method we deduced the well-known Casimir force between two parallel conducting planes in position as well as in momentum space.

Transferring our considerations to Casimir-Polder problems, we then explained the field theoretical treatment for a fluctuating electromagnetic field bounded by arbitrarily structured dielectric surfaces. We showed that the result of Casimir and Polder [4] for the potential energy of an atom in front of a plane with diverging dielectric constant can be derived by the thinning of a dielectric surface. In this context we deduced that the trace log formula of the Casimir energy simplifies considerably in the case of Casimir-Polder type problems, since only one cycle of fluctuation propagations has to be evaluated.

For the desired setup of corrugated surfaces, though, we argued that the thinning of one plate is not a favourable technique since the information of the position of the atom with respect to the ridges cannot be extracted. Still, the method could be of use in the consideration of surface roughness effects since there only the averaged potential induced by the presence of the plate is of relevance.

For the purpose of extracting the exact position of the atom with respect to the direction of the surface corrugation, we then substituted one of the surfaces by a sphere in our two surface setup. In this context, we first studied the potential induced by a scalar Dirichlet field for a sphere-plane configuration in the Casimir-Polder limit and confirmed recent results on the Casimir-Polder force that were obtained by the use of different calculational techniques [24, 41]. In the process of this calculation we showed that the integrations necessary for the evaluation of the potential become trivial for

the atom-side in the Casimir-Polder limit and derived an expression for the Casimir-Polder energy where only the integrations over the plate-side remain.

We then applied our result to the case of nontrivially shaped surfaces and derived a simple expression allowing for the numerically exact computation of the scalar Dirichlet Casimir-Polder potential for uniaxially corrugated surfaces. We argued that the formulation is non-perturbative in nature and can therefore probe regions that are arbitrarily close to the surface.

Consequently, we presented a possible numerical implementation and applied it exemplarily to the situation of a sinusoidal corrugation. The behaviour of the Casimir-Polder potential was studied for varying ratios between mean separation and corrugation amplitude along the direction of corrugation. Moreover, we considered the deviation of the potential strength for the corrugated surface with respect to the planar situation above a structure trough and above an inflexion point of the structure. These studies were performed for three different frequencies of the structure function.

Improvements of the presented work and extensions to it are possible in several directions.

First of all, a customized numerical implementation of the presented formulae for arbitrary corrugations can circumvent the limitations that are met within our implementation using MATHEMATICA. A faster algorithm could then be used to study more elaborate structure functions or even two-dimensional corrugations. As outlined, also the study of edge effects is possible within the formulation.

Furthermore several analytical extensions seem feasible. As already mentioned, an upgrade to scalar Neumann fields faces presumably no principle obstruction. Also it would evidently be of great interest to extend the calculations to the situation of a fluctuating gauge field in the presence of surfaces with arbitrary dielectric functions. This would provide the means of an explicit comparison to existing experimental data as outlined in the introduction of this thesis. Moreover, the inclusion of finite temperature effects in the considered sphere-surface configuration seems to be a worthwhile task [43].

All in all it is fair to say that even sixty years after Casimir's seminal prediction [1] the field of fluctuation-induced phenomena still harbours many unanswered questions.

A Propagators for the flat surface scenario

A.1 Inverse propagator on a plane

In order to proof Eq. (2.28), we have to show that

$$2\sqrt{-\nabla^2}G(\underline{x}) = \delta(\underline{x}) \tag{A.1}$$

is solved by the Green's function for ∂^2 with the x_3-component evaluated on a plane.

By transforming (A.1) to momentum space we find $G(\underline{p}) = \frac{1}{2|\underline{p}|}$ and therefore

$$G(\underline{x}) = \int \frac{\mathrm{d}^3 p}{(2\pi)^3} \frac{1}{2|\underline{p}|} e^{-\imath \underline{p}\underline{x}} \ . \tag{A.2}$$

Using a proper time representation for $G(\underline{p})$, we can write (A.2) as

$$G(\underline{x}) = \int \frac{\mathrm{d}^3 p}{(2\pi)^3} \left(\frac{1}{2\sqrt{\pi}} \int_0^\infty \frac{\mathrm{d}T}{\sqrt{T}} e^{-\underline{p}^2 T} \right) e^{-\imath \underline{p}\underline{x}} \ . \tag{A.3}$$

Upon completion of the square in $\underline{p}$ in the exponential, the integrations over the momenta can be performed and one gets

$$G(\underline{x}) = \int_0^\infty \mathrm{d}T \frac{1}{16\pi^2 T^2} \exp\left[-\frac{\underline{x}^2}{4T} \right] \ . \tag{A.4}$$

Evaluating the T-integration yields

$$G(\underline{x}) = \frac{1}{4\pi^2 \underline{x}^2} \ , \tag{A.5}$$

which in fact is the propagator on a flat surface parallel to the $x_1 - x_2$ plane (cf. Eq. (2.9)).

A.2 Half and full propagation circles

For the evaluation of the combined propagator $\mathcal{M}_{11}^{-1}\mathcal{M}_{12}$, it is feasible to choose $\mathcal{M}_{11}$ again in its Fourier representation. We thus have to evaluate the expression

$$\Delta\mathcal{M}_{12}(\underline{x} - \underline{x}') = \int_{\underline{p}} \int_{\underline{x}''} \frac{1}{(2\pi)^3} \frac{1}{4\pi^2} 2|\underline{p}| e^{-\imath \underline{p}(\underline{x} - \underline{x}'')} \frac{1}{(\underline{x}'' - \underline{x}')^2 + H^2} \ . \tag{A.6}$$

After a shift in the integration variable $\underline{x}'' \to \underline{x}'' + \underline{x}'$, the propagator reads

$$\Delta\mathcal{M}_{12}(\underline{x} - \underline{x}') = \frac{1}{16\pi^5} \int_{\underline{p}} |\underline{p}| e^{-\imath \underline{p}(\underline{x} - \underline{x}')} \int_{\underline{x}''} e^{\imath \underline{p}\underline{x}''} \frac{1}{(\underline{x}'')^2 + H^2} \ , \tag{A.7}$$

and now allows for the spatial integration to be carried out. One finds that

$$\Delta\mathcal{M}_{12}(\underline{x}-\underline{x}') = \frac{1}{8\pi^3}\int_{\underline{p}} e^{-|\underline{p}|H} e^{-\imath\underline{p}(\underline{x}-\underline{x}')} \ , \tag{A.8}$$

which upon integration over $\underline{p}$ reduces to

$$\Delta\mathcal{M}_{12}(\underline{x}-\underline{x}') = \frac{1}{\pi^2}\frac{H}{(H^2+(\underline{x}-\underline{x}')^2)^2} \ , \tag{A.9}$$

as given in Eq. (2.30).

At last, we want to evaluate the expression for one full propagation cycle $\Delta\mathcal{M}_{12}\Delta\mathcal{M}_{21}$ between plane surfaces. Using (A.9), we have to evaluate

$$\left[\Delta\mathcal{M}_{12}\Delta\mathcal{M}_{21}\right](\underline{x}-\underline{x}'') = \int_{\underline{x}'}\frac{1}{\pi^4}\frac{H}{(H^2+(\underline{x}-\underline{x}')^2)^2}\frac{H}{(H^2+(\underline{x}'-\underline{x}'')^2)^2} \ . \tag{A.10}$$

With a shift in the integration variable $\underline{x}' \to \underline{x}'+\underline{x}$, one finds

$$\left[\Delta\mathcal{M}_{12}\Delta\mathcal{M}_{21}\right](\underline{x}-\underline{x}'') = \int_{\underline{x}'}\frac{1}{\pi^4}\frac{H}{(H^2+\underline{x}'^2)^2}\frac{H}{(H^2+(\underline{x}'+\underline{y})^2)^2} \ , \tag{A.11}$$

where $\underline{y} \equiv \underline{x}-\underline{x}''$. The integral over the three components of $\underline{x}'$ can be rewritten as:

$$\begin{aligned}\left[\Delta\mathcal{M}_{12}\Delta\mathcal{M}_{21}\right](\underline{x}-\underline{x}'') = \frac{2H^2}{\pi^3}\int_0^\infty \frac{\underline{x}'^2}{(H^2+\underline{x}'^2)^2}\mathrm{d}x' \\ \times\int_{-1}^{1}\frac{1}{(H^2+\underline{x}'^2+\underline{y}^2+2|\underline{x}||\underline{y}|u)^2}\mathrm{d}u \ .\end{aligned} \tag{A.12}$$

Upon evaluation of the two remaining integrations and the resubstitution $\underline{y} \to \underline{x}-\underline{x}''$ we get the expression as given in Eq.(2.31)

$$\left[\Delta\mathcal{M}_{12}\Delta\mathcal{M}_{21}\right](\underline{x}-\underline{x}'') = \frac{2}{\pi^2}\frac{H}{(4H^2+(\underline{x}-\underline{x}'')^2)^2} \ . \tag{A.13}$$

B Field theory for dielectric boundaries

This appendix follows closely Refs. [37, 38]. Note, though, that a different sign convention is used regarding the Fourier transforms. Throughout this thesis we choose:

$$\begin{aligned} f(x) &= \int \frac{\mathrm{d}p}{2\pi} \tilde{f}(p) e^{-\imath p x} \\ \tilde{f}(p) &= \int \mathrm{d}x f(x) e^{\imath p x} \end{aligned} \tag{B.1}$$

B.1 Restriction of the partition function

Similar to the calculations of section 2.1, a partition function for fluctuating electromagnetic fields can be installed, where the required boundary conditions on the dielectric surfaces are implemented through a δ functional constraint. The main difference of the formulation for dielectric surfaces as compared to the treatment for scalar fields is - besides of course the extra field degrees of freedom coming with the vector potential A_μ - that the boundary conditions here are set up non-locally. This means that besides the arbitrarily shaped physical surfaces S_α, two flat auxiliary surfaces R_α are introduced on which the boundary conditions for the field components are implemented.

The setup is as follows: The surface S_1 of the dielectric medium with dielectric constant ϵ_1 is located at $x_3 = 0$, whereas the surface S_2 of the second dielectric medium sits at $x_3 = H$. The space between them is assumed to be vacuum (i.e. $\epsilon = 1$).

The configuration of both[20] surfaces should be such that their extensions in x_3-direction are parametrized by height functions $h_\alpha(\vec{x}_\parallel)$ with $\vec{x}_\parallel = (x_1, x_2)$. The two corresponding auxiliary surfaces R_α are placed at a distance $\pm L$ with L sufficiently large such that there is no intersection with the physical surfaces (see Figure B.1). The final result for the Casimir energy will of course not depend on the choice of L.

The derivation of the three non-local boundary conditions for the fluctuating field on the dielectric surfaces is given in B.2.

The starting point of the formulation is the generating functional for free

[20]Note, that the setup as chosen here is therefore not straightly conferable to the case where one of the surfaces is assumed to be a sphere (cf. section 4)

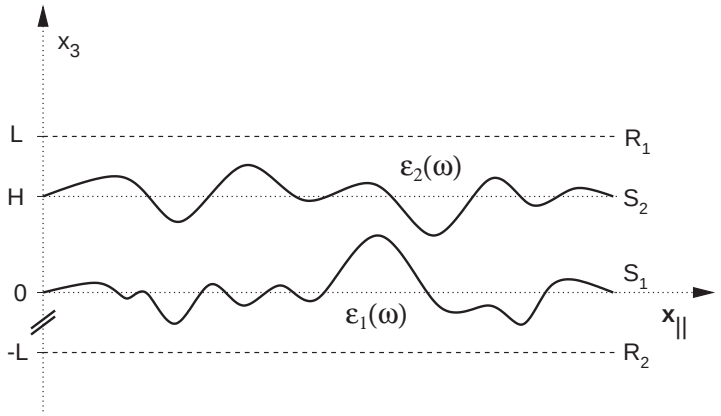

Figure 8: The two dielectric media bounded by their surfaces S_α are filling two half spaces. Their mean separation is H. With each physical surface S_α comes an auxiliary surface R_α on which the boundary conditions are implemented. This figure is taken from [37].

fields. For a complex-valued[21] gauge field A_μ it reads

$$\mathcal{Z}_0^2 = \int \mathcal{D}\,(A^\star A)\, e^{-S_{\rm E}(A^\star, A)} \ . \tag{B.2}$$

As before, it is convenient to work in a Euclidean time formulation. In Minkowski space one initially has the action

$$S(A^\star, A) = -\frac{1}{2}\int_x (F^\star_{\mu\nu} F^{\mu\nu})(x) - \frac{1}{\xi}\int_x (\partial_\mu A^{\star\mu})(\partial_\mu A^\nu)(x) \ , \tag{B.3}$$

with four-vectors $x = (t, \vec{x}_\parallel, x_3)$. The terms in (B.3) differ by a factor of $\frac{1}{2}$ from the usual QED Lagrangian for real valued fields and thereby assure that the correct photon propagator is obtained. The second term arises from the Fadeev-Popov gauge fixing procedure with the parameter ξ allowing for a switch between different gauges. In Feynman gauge (i.e. $\xi = 1$), the Euclidean action corresponding to Eq. (B.3) reads in momentum space

$$S_{\rm E}(A^\star, A) = \frac{1}{\beta}\sum_{n=-\infty}^{\infty} \frac{1}{(2\pi)^3}\int_{\vec{k}} A^{\star\mu}(\zeta_n, \vec{k}) G_{{\rm E},\mu\nu}(\zeta_n, \vec{k}) A^\nu(\zeta_n, \vec{k}) \ , \tag{B.4}$$

where finite temperature is accounted for by the introduction of bosonic Matsubara frequencies $\zeta_n = \frac{2\pi n}{\beta}$ and $\beta = \frac{1}{T}$. The associated Euclidean Green's function is given by $G_{{\rm E},\mu\nu}(\zeta, \vec{k}) = \delta_{\mu\nu} G(\zeta, \vec{k}) = (\zeta^2 + \vec{k}^2)^{-1}$.

[21] The complex-valued field is introduced for calculational convenience and has no physical implications.

With these prerequisites, the restricted functional integral is given by

$$\mathcal{Z}^2_{\mathrm{B.C.}}(H) = \frac{1}{\mathcal{Z}_0^2} \int \mathcal{D}(A^\star A) \prod_{\alpha,j} \prod_{\zeta_n} \prod_{\vec{x}\in R_\alpha} \times \delta \left[\int_{\vec{x}'\in S_\alpha} \mathcal{L}_{\alpha j\mu}(\zeta_n;\vec{x},\vec{x}') A^\mu(\zeta_n,\vec{x}') \right] e^{-S_{\mathrm{E}}(A^\star,A)} \ , \quad \text{(B.5)}$$

where $\mathcal{Z}_0$ again is the value of the integral over the unrestricted fields. The operator matrices $\mathcal{L}_{\alpha j\mu}$ implement the three $j = (1,2,3)$ boundary conditions on the vector potential that are induced by the properties of the two dielectric media bounded by their surfaces S_α. Their actual form is derived in B.2.

As this formulation allows for finite temperature, the Casimir free energy per unit area is given by

$$\mathcal{F}(H) = -\frac{\hbar c}{A\beta} \ln \left[\mathcal{Z}_{B.C.}(H) \mathcal{Z}_\infty^{-1}(H) \right] \ . \quad \text{(B.6)}$$

B.2 Implementation of the boundary conditions

In order to implement the boundary conditions for the electric and magnetic field on the dielectric surfaces, an equivalent reformulation of the optical extinction theorem is considered [44] which enforces the proper dielectric boundary conditions non-locally.

Inside a dielectric medium with a general frequency-dependent dielectric function $\epsilon(\omega)$ occupying a volume V with surface S, the magnetic field $\vec{B}$ obeys the Helmholtz wave equation reading

$$\left[\nabla^2 + \epsilon(\omega)\omega^2 \right] \vec{B}(\omega,\vec{x}) = 0 \ , \quad \text{(B.7)}$$

as follows directly from Maxwell's equations.

The free Green's function inside the dielectric medium consequently satisfies

$$\left[\nabla'^2 + \epsilon(\omega)\omega^2 \right] G^\epsilon(\omega;\vec{x},\vec{x}') = \delta^{(3)}(\vec{x}-\vec{x}') \ . \quad \text{(B.8)}$$

Equations (B.7) and (B.8) can then be combined into one equation and integrated over $\vec{x}'$ in a manner that Green's theorem can be applied to G^ϵ and the components of $\vec{B}$.

One finds that the following has to hold:

$$\int_{\vec{x}'\in S} \left[G^\epsilon(\omega;\vec{x},\vec{x}')(\hat{\boldsymbol{n}}'\nabla')\vec{B}(\omega,\vec{x}') - \vec{B}(\omega,\vec{x}')(\hat{\boldsymbol{n}}'\nabla' G^\epsilon(\omega;\vec{x},\vec{x}')) \right] = \begin{cases} \vec{B}(\omega,\vec{x}) & ,\vec{x}\in V \\ 0 & ,\vec{x}\notin V \end{cases} \ , \quad \text{(B.9)}$$

where the normal unit vector $\hat{\boldsymbol{n}}$ of the surface points into the vacuum. This equation is considered for the case where the coordinate vector $\vec{x}$ is located outside of the medium and therefore the integral on the left hand side of Eq. (B.9) has to vanish. This condition can now be rewritten into a form suitable for the derivation of the operators in Eq. (B.5) through a succession of vector identities [36].

Finally one has

$$\int_{\vec{x}'\in S}\Big[-\imath\omega\epsilon(\omega)(\hat{\boldsymbol{n}}'\times\vec{E}(\omega,\vec{x}'))+(\hat{\boldsymbol{n}}'\vec{B}(\omega,\vec{x}'))\nabla'+(\hat{\boldsymbol{n}}'\times\vec{B}(\omega,\vec{x}'))\times\nabla'\Big] \times G^{\epsilon}(\omega;\vec{x},\vec{x}')=0\ . \quad \text{(B.10)}$$

Now the argument goes as follows: the general continuity conditions for an electromagnetic field at a dielectric boundary without surface charges or surface currents state, that the tangential component of the electric as well as the normal and tangential component of the magnetic field are continuous across the surface. Therefore, Eq.(B.10) can be used as a boundary condition for the vacuum side of the surface (note that Eq. (B.10) does not contain the normal component of the electric field).

The condition (B.10) now determines the form of the operators $\mathcal{L}_{\alpha j\mu}(\zeta,\vec{x},\vec{x}')$ appearing in the restricted partition function of Eq. (B.5). Since the operators $\mathcal{L}_{\alpha j\mu}(\zeta,\vec{x},\vec{x}')$ act on the components of the vector potential and not the electromagnetic fields themselves, we have to express the condition (B.10) in terms of the gauge field.

The relation between the electric and magnetic field components with the components of the vector potential reads in Euclidean space:

$E_j=-\zeta A^j-\imath\partial_j A^0$ and $B_j=\epsilon_{jkl}\partial_k A^l$.

After a decomposition of the operators $\mathcal{L}_{\alpha j\mu}(\zeta,\vec{x},\vec{x}')=\hat{\boldsymbol{n}}_{\alpha k}(\vec{x}')\mathcal{L}^k_{\alpha j\mu}(\zeta,\vec{x},\vec{x}')$ with respect to the components normal vectors of the surfaces S_α one finds:

$$\mathcal{L}^1_\alpha(\zeta,\vec{x},\vec{x}')= \begin{pmatrix} 0 & -\frac{1}{\zeta\epsilon_\alpha}[\bar\partial_3\partial_2-\bar\partial_2\partial_3] & \frac{1}{\zeta\epsilon_\alpha}[\bar\partial_1\partial_3+\bar\partial_3\partial_1] & -\frac{1}{\zeta\epsilon_\alpha}[\bar\partial_1\partial_2+\bar\partial_2\partial_1] \\ \imath\partial_3 & -\frac{1}{\zeta\epsilon_\alpha}\bar\partial_1\partial_3 & \frac{1}{\zeta\epsilon_\alpha}\bar\partial_2\partial_3 & \zeta-\frac{1}{\zeta\epsilon_\alpha}[\bar\partial_2\partial_2-\bar\partial_1\partial_1] \\ -\imath\partial_2 & \frac{1}{\zeta\epsilon_\alpha}\bar\partial_1\partial_2 & -\zeta+\frac{1}{\zeta\epsilon_\alpha}[\bar\partial_3\partial_3-\bar\partial_1\partial_1] & -\frac{1}{\zeta\epsilon_\alpha}\bar\partial_3\partial_2 \end{pmatrix} \times G^{\epsilon_\alpha}_{\mathrm{E}}(\zeta;\vec{x}-\vec{x}') \quad \text{(B.11)}$$

$$\mathcal{L}^2_\alpha(\zeta,\vec{x},\vec{x}') = \begin{pmatrix} -\imath\partial_3 & -\frac{1}{\zeta\epsilon_\alpha}\bar{\partial}_1\partial_3 & \frac{1}{\zeta\epsilon_\alpha}\bar{\partial}_2\partial_3 & -\zeta+\frac{1}{\zeta\epsilon_\alpha}[\bar{\partial}_1\partial_1-\bar{\partial}_2\partial_2] \\ 0 & -\frac{1}{\zeta\epsilon_\alpha}[\bar{\partial}_2\partial_3+\bar{\partial}_3\partial_2] & -\frac{1}{\zeta\epsilon_\alpha}[\bar{\partial}_1\partial_3-\bar{\partial}_3\partial_1] & \frac{1}{\zeta\epsilon_\alpha}[\bar{\partial}_2\partial_1+\bar{\partial}_1\partial_2] \\ \imath\partial_1 & \zeta-\frac{1}{\zeta\epsilon_\alpha}[\bar{\partial}_3\partial_3-\bar{\partial}_2\partial_2] & -\frac{1}{\zeta\epsilon_\alpha}\bar{\partial}_2\partial_1 & \frac{1}{\zeta\epsilon_\alpha}\bar{\partial}_3\partial_1 \end{pmatrix} \times G^{\epsilon_\alpha}_{\mathrm{E}}(\zeta;\vec{x}-\vec{x}') \quad \text{(B.12)}$$

$$\mathcal{L}^3_\alpha(\zeta,\vec{x},\vec{x}') = \begin{pmatrix} \imath\partial_2 & \frac{1}{\zeta\epsilon_\alpha}\bar{\partial}_1\partial_2 & \zeta-\frac{1}{\zeta\epsilon_\alpha}[\bar{\partial}_1\partial_1-\bar{\partial}_3\partial_3] & -\frac{1}{\zeta\epsilon_\alpha}\bar{\partial}_3\partial_2 \\ -\imath\partial_1 & -\zeta+\frac{1}{\zeta\epsilon_\alpha}[\bar{\partial}_2\partial_2-\bar{\partial}_3\partial_3] & -\frac{1}{\zeta\epsilon_\alpha}\bar{\partial}_2\partial_1 & \frac{1}{\zeta\epsilon_\alpha}\bar{\partial}_3\partial_1 \\ 0 & \frac{1}{\zeta\epsilon_\alpha}[\bar{\partial}_3\partial_2+\bar{\partial}_2\partial_3] & -\frac{1}{\zeta\epsilon_\alpha}[\bar{\partial}_3\partial_1+\bar{\partial}_1\partial_3] & -\frac{1}{\zeta\epsilon_\alpha}[\bar{\partial}_2\partial_1-\bar{\partial}_1\partial_2] \end{pmatrix} \times G^{\epsilon_\alpha}_{\mathrm{E}}(\zeta;\vec{x}-\vec{x}') \quad \text{(B.13)}$$

with the barred partial derivatives acting on the spatial components of the Euclidean Green's function *inside* the dielectric media (cf. Eq.(B.8)), while the unbarred partial derivatives act on the gauge field itself.

B.3 Derivation of the trace log formula

Resembling the derivation in the scalar case (cf. section (2.1)), now three auxiliary fields $\psi_{\alpha j}(\zeta,\vec{x}_\parallel)$, $(j=1,2,3)$ corresponding to the three boundary conditions are introduced in order to perform the functional integral over the gauge fields. However, the auxiliary fields here are complex-valued since the arguments of the δ functions are complex-valued in this formulation. Furthermore, owing to the fact that the positions of the boundary conditions are located outside of the physical surfaces S_α, the auxiliary fields are defined on the surfaces R_α at $x_3 = L_\alpha = (-1)^{\alpha-1}L$.

The functional constraints for fixed α and j now read

$$\prod_{\zeta_n}\prod_{\vec{x}\in R_\alpha}\delta\left[\int_{\vec{x}'\in S_\alpha}\mathcal{L}_{\alpha j\mu}(\zeta_n;\vec{x},\vec{x}')A^\mu(\zeta,\vec{x}')\right] = \int\mathcal{D}[\psi^\star_{\alpha j}\psi_{\alpha j}] \times\exp\left[\imath\sum_n\int_{\vec{x}_\parallel}\int_{\vec{x}'\in S_\alpha}\left(\psi^\star_{\alpha j}(\zeta_n,\vec{x}_\parallel)\mathcal{L}_{\alpha j\mu}(\zeta_n;(\vec{x}_\parallel,L_\alpha),\vec{x}')A^\mu(\zeta_n,\vec{x}')+\text{c.c.}\right)\right]. \quad \text{(B.14)}$$

Upon insertion of the representation (B.14) into Eq.(B.5), the squares in the gauge fields can be completed and the integration $\int\mathcal{D}(A^\star A)$ over the vector

potential can be performed. The value of the integral over the free fields is absorbed into $\mathcal{Z}_0^2$. Eq. (B.5) then reads

$$\mathcal{Z}^2_{\mathrm{B.C.}}(H) = \int \prod_{\alpha j} \mathcal{D}\left[\psi^\star_{\alpha j}\psi_{\alpha j}\right] e^{-\tilde{S}[\psi^\star_{\alpha j},\psi_{\alpha j}]} \tag{B.15}$$

with the action

$$\tilde{S}[\psi^\star_{\alpha j},\psi_{\alpha j}] = \sum_{n,n'}\int_{\vec{x}_\parallel}\int_{\vec{x}'_\parallel} \psi^\star_{\alpha j}(\zeta_n,\vec{x}_\parallel)\mathcal{M}^{jl}_{\alpha\beta}(\zeta_n,\vec{x}_\parallel;\zeta_{n'},\vec{x}'_\parallel)\psi_{\beta l}(\zeta_{n'},\vec{x}'_\parallel)\ . \tag{B.16}$$

Due to the diagonality of $G_{\mathrm{E},\mu\nu}$ in its Lorentz indices, the matrix entries can be written as

$$\begin{aligned}\mathcal{M}^{jl}_{\alpha\beta}(\zeta,\vec{x}_\parallel;\zeta,\vec{x}'_\parallel) &= 2\pi\delta(\zeta-\zeta')\\ \times\int_{\vec{y}\in S_\alpha}\int_{\vec{y}'\in S_\beta}&\mathcal{L}_{\alpha j\mu}(\zeta;(\vec{x}_\parallel,L_\alpha),\vec{y})\mathcal{L}^\dagger_{\beta\mu l}(\zeta';(\vec{x}_\parallel,L_\beta),\vec{y}')G(\zeta;\vec{y}-\vec{y}')\ ,\end{aligned} \tag{B.17}$$

where $G(\zeta,\vec{y})$ is the photon propagator in vacuum. Since the auxiliary surfaces are chosen to be flat, this expression can further be simplified. Separating the Green's functions in the operators of Eqs. (B.11), (B.12) and (B.13) through $\mathcal{L}^k_\alpha(\zeta;\vec{x},\vec{y}) \equiv \mathsf{L}^k_\alpha(\zeta)G^{\epsilon_\alpha}_{\mathrm{E}}(\zeta;\vec{x}-\vec{y})$, Eq. (B.17) reads

$$\begin{aligned}\mathcal{M}^{jl}_{\alpha\beta}(\zeta,\vec{x}_\parallel;\zeta,\vec{x}'_\parallel) = 2\pi\delta(\zeta-\zeta')\int_{\vec{y}\in S_\alpha}\int_{\vec{y}'\in S_\beta}&\hat{\boldsymbol{n}}_{\alpha k}\hat{\boldsymbol{n}}'_{\beta s}[\mathsf{L}^k_\alpha\mathsf{L}^{'\dagger s}_\beta]_{jl}\\ \times G^{\epsilon_\alpha}_{\mathrm{E}}(\zeta;\vec{x}-\vec{y})|_{x_3=L_\alpha}&G^{\epsilon_\beta}_{\mathrm{E}}(\zeta';\vec{x}'-\vec{y}')|_{x'_3=L_\beta}G(\zeta;\vec{y}-\vec{y}')\ .\end{aligned} \tag{B.18}$$

Now the diagonality of the material Green's functions in their lateral coordinates is utilized. With the partially Fourier transformed propagator

$$G^{\epsilon_\alpha}_{\mathrm{E}}(\zeta;\vec{k}_\parallel,z) = \frac{\exp[-P_\alpha(\zeta,\vec{k}_\parallel)|z|]}{2P_\alpha(\zeta,\vec{k}_\parallel)} \tag{B.19}$$

where $P_\alpha(\zeta,\vec{k}_\parallel) = \sqrt{\epsilon_\alpha(\imath\zeta)\zeta^2+\vec{k}^2_\parallel}$, the barred derivatives acting on the spatial components of the propagators inside the materials can be performed and the operators L^k_α now take the form as given in Eqs. (3.6-3.8). The propagators of Eq. (B.18) then read

$$\begin{aligned}\mathcal{M}^{jl}_{\alpha\beta}(\zeta,\vec{k}_\parallel;\zeta',\vec{k}'_\parallel) = 2\pi\delta(\zeta-\zeta')\int_{\vec{y}\in S_\alpha}\int_{\vec{y}'\in S_\beta}&e^{\imath\vec{k}_\parallel\vec{y}_\parallel-\imath\vec{k}'_\parallel\vec{y}'_\parallel}\\ \times\frac{e^{-P_\alpha(\zeta,\vec{k}_\parallel)|L_\alpha-y_3|}}{2P_\alpha(\zeta,\vec{k}_\parallel)}&\frac{e^{-P_\beta(\zeta',\vec{k}'_\parallel)|L_\beta-y'_3|}}{2P_\beta(\zeta',\vec{k}'_\parallel)}\\ \times\hat{\boldsymbol{n}}_{\alpha k}\hat{\boldsymbol{n}}'_{\beta s}[\hat{\mathsf{L}}^k_\alpha(\zeta,\vec{k}_\parallel)&\hat{\mathsf{L}}^{'\dagger s}_\beta(\zeta',\vec{k}'_\parallel)]_{jl}G(\zeta;\vec{y}-\vec{y}')\ ,\end{aligned} \tag{B.20}$$

with the surface normal vectors given as

$$\hat{\boldsymbol{n}}_\alpha = \frac{(-1)^\alpha}{\sqrt{g_\alpha}} \begin{pmatrix} \partial_1 h(y_\parallel) \\ \partial_2 h(y_\parallel) \\ -1 \end{pmatrix} . \tag{B.21}$$

The factor in the denominator is the square root of the induced surface metric: $\sqrt{g_\alpha} = \sqrt{1 + (\partial_1 h(y_\parallel))^2 + (\partial_2 h(y_\parallel))^2}$.

The physical quantities should of course not depend on the choice of the distance L where the auxiliary surfaces are located. Rewriting $|L_\alpha - y_3| = (-1)^{\alpha-1}(L_\alpha - y_3)$, one sees that the matrix entries $\mathcal{M}^{jl}_{\alpha\beta}(\zeta, \vec{k}_\parallel; \zeta', \vec{k}'_\parallel)$ factorize. One has

$$\mathcal{M}^{jl}_{\alpha\beta}(\zeta, \vec{k}_\parallel; \zeta', \vec{k}'_\parallel) = \eta^\alpha(\zeta, \vec{k}_\parallel) \tilde{\mathcal{M}}^{jl}_{\alpha\beta} \eta^\beta(\zeta', \vec{k}'_\parallel) , \tag{B.22}$$

with the functions $\eta^\alpha(\zeta, \vec{k}_\parallel) = \exp\left(-P_\alpha(\zeta, \vec{k}_\parallel)L\right)/2P_\alpha(\zeta, \vec{k}_\parallel)$ and the modified propagator matrix

$$\begin{aligned} \tilde{\mathcal{M}}^{jl}_{\alpha\beta}(\zeta, \vec{k}_\parallel; \zeta', \vec{k}'_\parallel) = 2\pi\delta(\zeta - \zeta') \int_{\vec{y}\in S_\alpha} \int_{\vec{y}'\in S_\beta} \\ \times e^{\imath\vec{k}_\parallel \vec{y}_\parallel - \imath\vec{k}'_\parallel \vec{y}'_\parallel} e^{-[(-1)^\alpha P_\alpha(\zeta,\vec{k}_\parallel) y_3 + (-1)^\beta P_\beta(\zeta', \vec{k}'_\parallel) y'_3]} \\ \times \hat{\boldsymbol{n}}_{\alpha k} \hat{\boldsymbol{n}}'_{\beta s} [\hat{\mathsf{L}}^k_\alpha(\zeta, \vec{k}_\parallel) \hat{\mathsf{L}}^{\prime\dagger s}_\beta(\zeta', \vec{k}'_\parallel)]_{jl} G(\zeta; \vec{y} - \vec{y}') . \end{aligned} \tag{B.23}$$

Since the action is quadratic in the auxiliary fields (cf. Eq.(B.16)), one sees immediately that $\mathcal{Z}(H) = \det{}^{-\frac{1}{2}} \mathcal{M}$, with the determinant running over the continuous momenta $(\zeta, \vec{k}_\parallel)$ and the discrete indices labelling the plates $\alpha = (1, 2)$ as well as the three boundary conditions $j = (1, 2, 3)$. Since the factors $\eta^\alpha(\zeta, \vec{k}_\parallel)$ are independent of the mean surface distance H, they drop out in the ratio of the restricted and unrestricted partition functions and therefore in the calculation of the free energy and force of the system.

The free energy per surface area now reads

$$\mathcal{F}(H) = \frac{\hbar c}{2A\beta} \ln\det\left(\tilde{\mathcal{M}}\tilde{\mathcal{M}}^{-1}_\infty\right) . \tag{B.24}$$

As we are performing our calculations for zero temperature, we work with

$$E_{cas}(H) = \frac{1}{2}\frac{\hbar c}{T_E} \mathsf{tr} \ln \mathcal{M}\mathcal{M}^{-1}_\infty \quad , \tag{B.25}$$

where we have dropped the $\sim$ for notational convenience.

Equation (B.25) together with the expression for the propagators

$$\mathcal{M}^{jl}_{\alpha\beta}(\zeta,\vec{k}_\parallel;\zeta',\vec{k}'_\parallel) = 2\pi\delta(\zeta-\zeta')\int_{\vec{y}\in S_\alpha}\int_{\vec{y}'\in S_\beta} \times e^{\imath\vec{k}_\parallel\vec{y}_\parallel-\imath\vec{k}'_\parallel\vec{y}'_\parallel}e^{-[(-1)^\alpha P_\alpha(\zeta,\vec{k}_\parallel)y_3+(-1)^\beta P_\beta(\zeta',\vec{k}'_\parallel)y'_3]} \times \hat{\boldsymbol{n}}_{\alpha k}\hat{\boldsymbol{n}}'_{\beta s}[\hat{\mathsf{L}}^k_\alpha(\zeta,\vec{k}_\parallel)\hat{\mathsf{L}}'^{\dagger s}_\beta(\zeta',\vec{k}'_\parallel)]_{jl}G(\zeta;\vec{y}-\vec{y}') \quad \text{(B.26)}$$

are now the starting point for our investigations in section 3.

C Numerical discretization parameters

C.1 Discretization parameters of the momentum integration

Figure 9 shows the course of $f(q)$ as defined in Eq.(5.25) corresponding to the set of spatial discretization parameters as chosen in Figs. 4 and 5. The dominant contribution of $f(q)$ to the Casimir-Polder energy for this set of parameters approximately lies at the value $q/H \approx 0.4$. Similar graphs are obtained when $f(q)$ is plotted with respect to the spatial parameters as used in Figs. 3, 6 and 7. Due to this behaviour we choose the parameters of the q-integration as $L_q = 0.01$, $R_q = 4$ and $\Delta q = 0.04$.

For precise numerical calculations of the Casimir-Polder potential, the values for the discretization parameters of the momentum integration have to be picked according to each used combination of the parameters of the spatial discretization. Also, Fig. 9 shows, that the choice of equidistant nodes N_q is not ideal. Here, obviously an adaptive algorithm selecting the nodes N_q according to the respective course of $f(q)$ for each set of spatial parameters would be desirable.

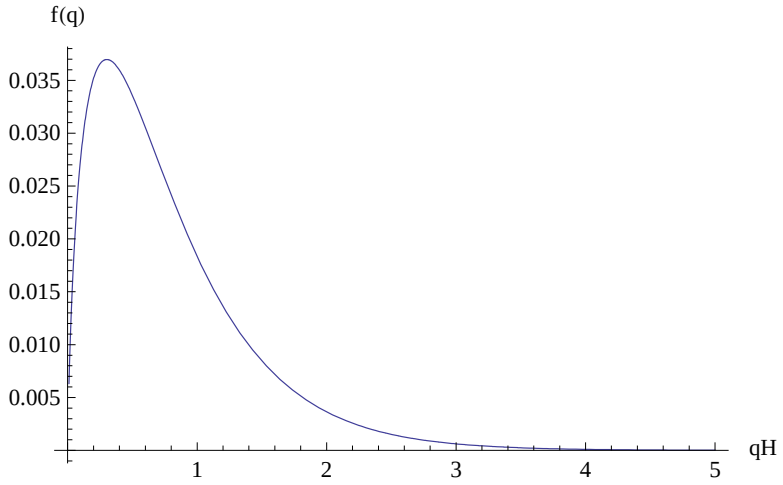

Figure 9: In this figure, the course of $f(q)$ as defined in Eq.(5.25) is shown for the parameters $A/H = 0.01$, $\omega/H = 1$, $L_x = 2$, $\Delta x/H = 0.05$ and $\Delta s/H = 0.025$ in the regime $0.01 \leq qH \leq 5$. It can be seen that the dominant contributions of $f(q)$ are peaked around $q/H \approx 0.4$ and decline quickly as $q/H \to \infty$. On the basis of this figure we use the following dimensionless parameters for our considerations of section 5.2.4: $L_q = 0.01$, $R_q = 4$ and $\Delta q = 0.04$.

C.2 Validity limits

In Table 1 we give an overview of the relative deviation of the Casimir-Polder potential as presented in Figures 4-7 from the corresponding analytical value in the flat surface limit. The agreement with the analytical result for planar structures is tested by choosing the amplitude of the corrugation small compared to the mean distance. To this end, we choose $A = 0.01H$. The relative deviation as given in the last row of Table 1 gives the combined error that is caused by the numerical implementation as presented in section 5.2.2.

Note, that the stated deviations hold for all distances between sphere and corrugated surface. In Figs. 4 and 5, where the value of α is studied along the direction of corrugation x, the displacement of the sphere is achieved by a continuous modulation of the structure function itself. Thus the error induced by the finite plate size L_x and the finite number of nodes N_x is equal for every point along x. In Figs. 6 and 7, where the behaviour of α is studied for a varying distance between surface and sphere, the edges of the surface L_x as well as the number of nodes N_x scale with the separation between surface and sphere such that the sphere always retains the same distance to the edges and always "sees" the same number of spatial discretization nodes as it approaches the corrugated surface.

Figure	N_x	$\alpha/\alpha_{\text{analytic}}$	deviation from the planar surface limit
4,5	80	1.005	0.5%
6	63	0.962	3.8%
7	126	0.960	4%

Table 1: This table states the deviation of the value for the potential strength parameter α as defined in Eq.(5.27) from the analytical value α_{analytic} in the planar case. The deviation is considered with respect to the number N_x of discretization nodes as used in the studies within Figs. 4-7. Note, that the obtained degree of deviation is not always lower for a higher number of discretization nodes N_x. This is due to the used discretization scheme as explained in section 5.2.2. An alternative discretization scheme that avoids this unwanted oscillatory behaviour is discussed in section 5.3.1.

References

[1] H. Casimir, On the attraction between two perfectly conducting plates, Proc. K. Ned. Akad. Wetensch. **51**, 793–795 (1948).

[2] S. K. Lamoreaux, Demonstration of the Casimir Force in the 0.6 to $6\mu m$ Range, Phys. Rev. Lett. **78**(1), 5–8 (Jan 1997).

[3] U. Mohideen and A. Roy, Precision Measurement of the Casimir Force from 0.1 to $0.9\mu m$, Phys. Rev. Lett. **81**(21), 4549–4552 (Nov 1998).

[4] H. B. Casimir and D. Polder, The Influence of Retardation on the London-van der Waals Forces, Phys. Rev. **73**(4), 360–372 (1948).

[5] P. Milloni, *The Quantum Vacuum*, Academic San Diego, 1994.

[6] H. B. Casimir, Sur les forces van der Waals-London, J. Chim. Phys. **46**, 407 (1949).

[7] M. Fisher and P. de Gennes, Phenomenes aux parois dans un melange binaire critique, Acad. Sci. Paris B **287**, 207 (1978).

[8] C. Hertlein, L. Helden, A. Gambassi, S. Dietrich, and C. Bechinger, Direct measurement of critical Casimir forces, Nature **451**(7175), 172–175 (Jan. 2008).

[9] H. B. Chan, V. A. Aksyuk, R. N. Kleiman, D. J. Bishop, and F. Capasso, Quantum Mechanical Actuation of Microelectromechanical Systems by the Casimir Force, Science **291**(5510), 1941–1944 (2001).

[10] M. Bordag, U. Mohideen, and V. Mostepanenko, New Developments in the Casimir Effect, Phys. Rep. **353**, 1 (2001).

[11] K. Milton, *The Casimir Effect*, World Scientific, 2001.

[12] V. Mostepanenko and N. Trunov, *The Casimir Effect and its Applications*, Oxford Science Publications, 1997.

[13] P. A. Martin and P. Buenzli, The Casimir Effect, Acta Phys. Polonica B **37**, 2503–2559 (2006).

[14] S. Y. Buhmann and D.-G. Welsch, Dispersion forces in macroscopic quantum electrodynamics, Prog. Quant. Electron. **31**, 51 (2007).

[15] B. V. Derjaguin, I. I. Abrikosova, and E. M. Lifshitz, Direct measurement of molecular attraction between solids separated by a narrow gap, Q. Rev. Chem. Soc. **10**, 295–329 (1956).

[16] J. Blocki, J. Randrup, W. Swiatecki, and C. Tsang, Proximity forces, Ann. Phys. **105**, 427–462 (1977).

[17] M. Schaden and L. Spruch, Infinity-free semiclassical evaluation of Casimir effects, Phys. Rev. A **58**(2), 935–953 (Aug 1998).

[18] H. Gies, K. Langfeld, and L. Moyaerts, Casimir effect on the worldline, JHEP **0306**(06), 018 (2003).

[19] L. Moyaerts, K. Langfeld, and H. Gies, Worldline approach to the Casimir effect, [arXiv:hep-th/0311168], 2003.

[20] R. L. Jaffe and A. Scardicchio, Casimir Effect and Geometric Optics, Phys. Rev. Lett. **92**(7), 070402 (Feb 2004).

[21] A. Scardicchio and R. Jaffe, Casimir Effects: An Optical Approach I. Foundations and Examples, Nucl. Phys. B **704**(3), 552–582 (Jan. 2005), [arXiv:quant-ph/0406041].

[22] H. Gies and K. Klingmüller, Casimir Effect for Curved Geometries: Proximity-Force-Approximation Validity Limits, Phys. Rev. Lett. **96**(22), 220401 (2006).

[23] M. Bordag, Casimir effect for a sphere and a cylinder in front of a plane and corrections to the proximity force theorem, Phys. Rev. D **73**(12), 125018 (2006).

[24] A. Bulgac, P. Magierski, and A. Wirzba, Scalar Casimir effect between Dirichlet spheres or a plate and a sphere, Phys. Rev. D **73**(2), 025007 (2006).

[25] T. Emig, N. Graham, R. L. Jaffe, and M. Kardar, Casimir Forces between Arbitrary Compact Objects, Phys. Rev. Lett. **99**(17), 170403 (2007).

[26] V. Druzhinina and M. DeKieviet, Experimental Observation of Quantum Reflection far from Threshold, Phys. Rev. Lett. **91**(19), 193202 (Nov 2003).

[27] V. Droujinina, On Quantum Reflection and The Casimir Effect, Dissertation, University of Heidelberg, 2003.

[28] U. Warring, Auf der Suche nach dem perfekten Quantenreflex, Diploma thesis, University of Heidelberg, 2006.

[29] V. B. Bezerra, G. L. Klimchitskaya, and C. Romero, Surface roughness contribution to the Casimir interaction between an isolated atom and a cavity wall, Phys. Rev. A **61**(2), 022115 (Jan 2000).

[30] D. A. Dalvit, P. A. M. Neto, A. Lambrecht, and S. Reynaud, Probing quantum vacuum geometrical effects with cold atoms, Phys. Rev. Lett. **100**, 040405 (2008).

[31] M. Bordag, D. Robaschik, and E. Wieczorek, Quantum field theoretic treatment of the Casimir effect, Ann. Phys. **165**, 192–213 (Nov. 1985).

[32] T. Emig, A. Hanke, R. Golestanian, and M. Kardar, Normal and lateral Casimir forces between deformed plates, Phys. Rev. A **67**(2), 022114 (Feb 2003).

[33] A. Hanke and M. Kardar, Correlation functions near modulated and rough surfaces, Phys. Rev. E **65**(4), 046121 (Apr 2002).

[34] R. Golestanian and M. Kardar, Path-integral approach to the dynamic Casimir effect with fluctuating boundaries, Phys. Rev. A **58**(3), 1713–1722 (Sep 1998).

[35] H. Li and M. Kardar, Fluctuation-induced forces between rough surfaces, Phys. Rev. Lett. **67**(23), 3275–3278 (Dec 1991).

[36] J. Jackson, *Classical Electrodynamics*, Wiley, 3rd edition, 1999.

[37] T. Emig and R. Büscher, Towards a theory of molecular forces between deformed media, Nucl. Phys. B **696**, 468–491 (2004).

[38] R. Büscher, Casimir Forces and Geometry, Dissertation, University of Cologne, 2005.

[39] E. Lifshitz, The Theory Of Molecular Attrative Forces Between Solids, Soviet Phys. JETP **2**, 73–83 (1956).

[40] J. F. Babb, G. L. Klimchitskaya, and V. M. Mostepanenko, Casimir-Polder interaction between an atom and a cavity wall under the influence of real conditions, Phys. Rev. A **70**(4), 042901 (Oct 2004).

[41] T. Emig, Fluctuation induced quantum interactions between compact objects and a plane mirror, [arXiv:cond-mat/0712.2199], 2007.

[42] M. Abramowitz and I. A. Stegun, *Handbook of Mathematical Functions With Formulas, Graphs, and Mathematical Tables*, National Bureau of Standards - Applied Mathematics Series 55, Dover, New York, tenth dover printing edition, 1964.

[43] K. Klingmüller and H. Gies, Geothermal Casimir Phenomena, [arXiv:0710.4473], 2007.

[44] A. Marvin and V. Celli, Relation between the surface impedance and the extinction theorem on a rough surface, Phys. Rev. B **50**(19), 14546–14553 (Nov 1994).